Preliminary thermal design of an earth-observation micro-satellite in SS LEO orbit with ESATAN-TMS

Mataix Caballero, Diego

Abstract

Thermal control systems are an essential part of every spacecraft design and operation. To maintain all the subsystems of a satellite within their operational temperature ranges presents a difficult challenge for every mission design. Furthermore, the thermal requirements and characteristics of a satellite vary greatly depending on the orbit and the payload requirements, hence there is not a one-fits-all solution. Therefore, the need for a tool to simulate the thermal performance of an object in orbit becomes apparent. For this study the software ESATAN-TMS, which relies on a CPU-based implementation of the Monte Carlo ray tracing technique, will be employed throughout for all simulations. The scope of this study is to carry out the preliminary thermal design for an earth-observation (EO) satellite in low-earth sun-synchronous (SS) circular orbit. The payload includes a IR telescope with a CCD IR detector, which must be cooled to a sufficiently low temperature as to provide minimum noise in the data gathered by the detector.

Key Words: Thermal Control Systems, Space Thermal Control; Conduction; Radiation; Numerical Simulation; Micro-satellite; ESATAN-TMS; Earth-Observation Satellite

---

Contents

List of Figures

List of Tables

1 Introduction

This preliminary design study consists in the modelling and simulation of the thermal design of an earth-observation (EO) satellite in low-earth sun-synchronous (SS) circular orbit. The payload includes a IR telescope with a CCD Infrared (IR) detector, which must be cooled to a sufficiently low temperature as to provide minimum noise in the data gathered by the detector, with the choice of it being cryogenically cooled or not. The impact of the choice of either an active or a passive thermal control design on the total power generation and dissipation of the satellite must be considered. Furthermore, a number of other satellite payloads are simulated, namely the electronic box, containing the On-Board-Data-Handling (OBDH) sub-system, the reaction wheels used for attitude control of the satellite, which is essential for the accurate pointing of the IR telescope, and a science instrument with a specified power dissipation.

All the components of the satellite must be kept within their operational temperature ranges for the whole duration of the orbit in all operational modes: nominal mode, survival mode, and in a cold case. In nominal mode all the instrumentation is powered on and, therefore, is the mode with the most heat dissipation, in survival mode only the OBDH system is dissipating half of its nominal power, and finally, in the cold case all instruments are powered off.

The preliminary design of this satellite will focus on the selection of geometry, materials, thickness of the various parts, thermo-optical coatings and finishes, use of radiators, heaters or other devices for the means of keeping the components within their operational parameters.

For this study the software ESATAN-TMS, which relies on a CPU-based implementation of the Monte Carlo ray tracing technique for its radiative analysis, will be employed throughout for all simulations. Due to the high computational cost of this method the least amount of nodes are chosen for this preliminary study, therefore, in parts of the satellite where there is not a steep temperature gradient, the number of nodes is kept to a minimum.

2 Methodology

This section intends to provide insight into the process that was used for the preliminary design of the EO satellite and the simulation of its thermal performance, for both the proposed design solutions. These two solutions are proposed due to the delicate nature of the CCD detectors such as those that will be employed in this study, as well as the low temperatures required to keep their performance at adequate levels, reducing the noise captured by the sensor.

The first solution that is proposed consists of a passive thermal control system, with the CCD detector being cooled with the use of radiators only. This presents key advantages compared to an active thermal control approach as in this case the ability to cool down the component is not limited to the moments when the active system can be powered and operating, therefore, this approach also involves a lower risk. However, due to the difficulty to approach cryogenic temperatures with a passive thermal design, a slight variation is proposed. In this second solution a cryo-cooler is used to maintain the CCD sensor at 70 K, allowing for minimum noise detected by the sensor. Due to the different operating conditions of the detector in both solutions, a different CCD sensor is proposed for each. Additionally, due to the added power consumption of the cryo-cooler the solar panels must be adequetely reconfigured to provide sufficient power, which also provides the challenge of managing the added

heat dissipation in the interior of the satellite.

2.1 Mission definition

The type of orbit and the instrumentation on-board the satellite have a severe impact on the thermal design, therefore, this section aims at providing an overview of the mission and its characteristics.

2.1.1 Orbit

The satellite operates in a LEO SS 12am circular orbit at a height of 800 km. The mission design was performed with STK mission analysis tool.

2.1.2 Instrumentation and payload

The design must be able to accommodate all of the payloads and instrumentation that have been modelled for this mission, as well as to maintain them within their operational limits. Table 1 shows a list of the payloads that are employed in this study, their dimensions, power consumption, operating temperature limits and manufacturer. It must be noted that the heat pipes and thermal straps are only modelled through user-defined conductors (UDC) and not with actual geometry.

Table 1: Table showing the chosen instrument payload configuration . Note that cryo-cooler is only employed in the active thermal control system configuration.

Payload ID	**Payload**	**Dimensions [mm^3]**	**Power Consumption [W]**	**Operating Temperature [K]**		**Manufaturer**	**Source**
				Min.	Max.		
PLD1	Experiment	60x60x30	2	333.15	253.15	N/A	N/A
PLD2	Reaction Wheels	70x70x25	4	233.15	343.15	Blue canyon	[1]
EBox	OBDH	150x150x40	16	248.15	338.15	Endurosat	[2]
N/A	Cryo-cooler	37.8x66.2x14.5	16	218.15	358.15	Ricor	[3]
N/A	Heat Pipe*	N/A	0	N/A	N/A	N/A	[4]
N/A	Thermal Strap	N/A	0	40	350	Thermal lynx	[5]

On the other hand, Table 2 shows the power dissipated by all instruments for each of the configurations proposed, the passive thermal control (PC) design and the active thermal control design (AC), as well as the total power dissipated under each configuration.

Table 2: Table showing information regarding the power dissipated by the various instruments and components, for both proposed thermal control system configurations.

Instrument	**Power Dissipated [W]**	
	PC config.	AC config.
PLD1	2	2
PLD2	4	4
OBDH	16	16
CCD	0.1	0.1
Cryo Diss	0	16
Total	22.1	38.1

Regarding, Table 3 shows the solar panel configurations for each of the proposed solutions. The solar panel area as well as the efficiency and packing factors were chosen to equal the power provided by the solar panels to the power dissipated by the various instruments.

Table 3: Table showing information regarding the solar panels for both proposed thermal control system configurations. The mean heat flux received by the solar panels is provided, together with the solar panel area, the efficiency and packing factors chosen as well as the power generated. Note that both configuration have different solar panel areas since the active + passive configuration requires additional power to run the cryo-cooler.

Cooling	**Mean Heat Flux [W/mˆ2]**	**Solar Panel Area [mˆ2]**	**Efficiency**	**Packing factor**	**Power Generated [W]**
Passive	602.67	0.21	0.25	0.7	22.1
Active + Passive	602.67	0.28	0.25	0.9	38.1

Finally, regarding the CCD sensor, as stated a different model is proposed for each configuration. For the passive thermal control system configuration, the CCD290-99 model manufactured by e2V is chosen. This CCD sensor provides great performance in the IR spectrum whilst maintain an operational temperature range between 153 K and 323 K, with the noise being minimum at 153 K, therefore the proposed passive thermal design will aim to reach that temperature [6]. Lastly, the active thermal control system, which will use a cryo-cooler to maintain the detector at 70 K uses an IR detector, uses a CCD manufactured by PICNIC which was proposed for the MIRIS infrared telescope [7]. This detector can operate in a range of temperatures between 60 K and 110 K. The cryo-cooler proposed is the Ricor K538 Model. Which has a minimum and maximum power consumption of 6 W and 16 W respectively and the cold tip is able to reach 65K to 110K [3].

2.2 ESATAN-TMS micro-satellite model.

Both of the proposed configurations are based on the same platform, which was configured in ESATAN-TMS, and share many similarities. Including materials and thermo-optical properties employed for all the components of the satellite. Part of the key characteristics of the thermal control system that has been proposed is the use of a V-shaped radiator in one of the sides of the spacecraft, which is composed of a conical baffle. A conical baffle is, due to its small opening, advantageous with respect to shielding off Earth radiation but it minimizes at the same time the view of the radiator to deep space. Therefore, a conical baffle for the telescope CCD sensor radiator with a high reflective inner surface and an opening angle such that most of the radiation incident to the inner surface is reflected back to space. This type of radiator is widely used for passive thermal control systems were extremely low operational temperatures are required [8].

2.2.1 Materials and thermo-optical properties

Table 4 and 5 show the materials that have been chosen for this preliminary design study. where Al-6061 was chosen for most of the structure as it provides adequate thermal performance while presenting good structural characteristics as well. As these surfaces were designed to have an anodised black finish, Al-7075 could not be used as the ECSS documentation prohibits this. Moreover, CFRP was chosen for areas were a low conductivity of the material was desirable, such as the trays for placing the various instruments and the telescope lens assembly.

Table 4: Table showing the isotropic materials that have been employed in this study, as well as the source from which the data was gathered.

Isotropic Materials				Source
Name	k [W/(m·K)]	C_p [J/(kg·K)]	ρ [kg/m^3]	
Al-6061	160	900	2700	[9]
Al-2219	121	864	2840	[9]
Al-7075	130	960	2810	[9]
Copper	385	385	7760	[9]
GaAs	55	1000	5300	[9]
Glass	59	310	5330	[9]
Silicon	124	794	2300	[9]
MLI foil	0	900	300	[9]

Table 5: Table showing the orthotropic materials that have been employed in this study, as well as the source from which the data was gathered.

Orthotropic Materials						Source
Name	k_1 [W/(m·K)]	k_2 [W/(m·K)]	k_3 [W/(m·K)]	C_p [J/(kg·K)]	ρ [kg/m^3]	
CFRP	42	42	5	800	1750	[9]

Table 6 shows the characteristics of the MLI depending on the temperature.

Table 6: Effective transversal thermal conductance for the MLI blankets, in terms of the temperature.

MLI_h_throught	
Temperature [ºC]	$h_{eff}[W/(m^2 \cdot K)]$
-75	0.00393
-45	0.01040
14	0.01499
50	0.02289
70	0.03368

Finally, Table 7 shows the thermo-optical properties for both the infrared and solar bands, of the coatings and finishes that are used in this preliminary desing.

Table 7: Table showing the thermo-optical properties of the coatings that have been employed in this study, as well as the source from which the data was gathered.

Name	**Infrared**				**Solar**				**Source**
	ε	τ	$\rho_{specular}$	$\rho_{diffuse}$	α	τ	$\rho_{specular}$	$\rho_{diffuse}$	
Al_anodized	0.60	0.00	0.00	0.40	0.20	0.00	0.00	0.80	[10]
Al_anodized_blck	0.85	0.00	0.00	0.15	0.90	0.00	0.00	0.10	[10]
Black_paint	0.90	0.00	0.00	0.10	0.90	0.00	0.00	0.10	[10]
Copper	0.05	0.00	0.00	0.95	0.90	0.00	0.00	0.10	[10]
White_paint	0.80	0.00	0.00	0.20	0.20	0.00	0.00	0.80	[10]
SSM	0.00	0.00	0.00	1.00	0.08	0.00	0.00	0.92	[10]
CCD	1.00	0.00	0.00	0.00	0.00	0.00	0.00	1.00	[10]
OSR	0.80	0.00	0.00	0.20	0.08	0.00	0.92	0.00	[10]
Solar_cells	0.75	0.00	0.00	0.25	0.75	0.00	0.00	0.25	[10]
IR_lens	0.10	0.90	0.00	0.00	0.10	0.00	0.00	0.90	[10]
Kapton_ITO	0.80	0.00	0.00	0.20	0.50	0.00	0.00	0.50	[10]
Goldised Kapton	0.02	0.00	0.00	0.98	0.25	0.00	0.00	0.75	[10]
VDA_Kapton	0.10	0.00	0.90	0.00	0.20	0.00	0.80	0.00	[10]

2.2.2 Radiative and Analysis case

The radiative case is set so that the satellite model is in the chosen orbit, with 12 orbital positions, with the correct pointing of its solar panels in the direction of the incident solar radiation, as to maximise the extracted power, and IR telescope. Furthermore, the analysis case is configured such that the simulation provides transient results with a cyclic solution. Special care is given to provide sufficient iterations as to arrive at a solution which converges.

2.3 ESATAN-TMS micro-satellite model. Passive thermal control system configuration

This section aims to provide a detailed description of the proposed configuration which uses a passive thermal control system to cool the CCD sensor.

2.3.1 Geometry

The components of the nodes and labels, as well as the geometry, materials and surfaces assigned to each of the elements and sub-elements that compose the satellite model are shown in Table 8 and Table 9 respectively.

Table 8: Table showing the elements and sub-elements that are used for the satellite with a completely passive thermal control system configuration. The labels specified in ESATAN-TMS and the nodes that compose each sub-element are shown too.

ELEMENT	SUB-ELEMENT	LABEL	NODE_i	NODE_f
Structure		BODY	10000	19999
	Panels	BODY_PANEL	10000	10999
	Instrument plate	BODY_PLATE_1	11000	11999
	Instrument plate	BODY_PLATE_2	12000	11999
Solar Panels		SPS	20000	29999
	Structure	SPS_STR	20000	20999
	Solar Cells	SPS_CELLS	21000	21999
Instruments		INS	30000	39999
	Electronic Box	INS_EB	30000	30999
	Payload 1	INS_PLD1	31000	31999
	Payload 2	INS_PLD2	32000	32999
IR Telescope		IR_TEL	40000	49999
	Structure	IR_TEL_STR	40000	40999
	Disk Structure	IR_TEL_STR_2	45000	45999
	IR Sensor	IR_TEL_CCD	41000	41999
	Telescope Assembly	IR_TEL_OBJ	43000	43999
	Lens	IR_TEL_LENS	44000	44999
MLI		MLI	50000	59999
	Exterior	MLI_EXT	50000	50999
	Telescope	MLI_IR_TEL	51000	51999
Radiator		RAD	60000	69999
	Instrument radiator	RAD_INS	60000	60999
	CCD radiator	RAD_IR_TEL	61000	61999
		RAD_IR_TEL_2	62000	62999
	Telescope assembly radiator	RAD_IR_Tel_STR	63000	63999
	Structure radiator	RAD_STR	64000	64999

Table 9: Table showing the geometry that is used to represent the different elements and systems of the satellite, as well as the materials and thermo-optical properties assigned to each geometry. For the case of the passive thermal control system for the IR telescope CCD sensor.

Element	Sub-element	Shape	Size x [m]	Size y [m]	Size z [m]	Thickness [m]	Surface 1	Surface 2	Material
Structure									
	Panels	Box	0.4	0.3	0.375	2.00E-03	Al_anodized_black	Al_anodized_black	Al_6061
	Instrument plate	Rectangle	0.4	0.3	N/A	2.00E-03	Black Paint	Black Paint	CFRP
	Instrument plate	Rectangle	0.4	0.3	N/A	2.00E-03	Black Paint	Black Paint	CFRP
Solar Panels		Rectangle	0.7	0.3	N/A	1.00E-03	Solar_cells	Kapton_ITO	GaAs/Al7075
	Structure								
	Solar Cells								
Instruments									
	Electronic Box	Box	0.15	0.15	0.04	2.00E-03	Black Paint	Black Paint	Al_2219
	Payload 1	Non-Geometrical Node	N/A	N/A	N/A	N/A	N/A	N/A	Al_6061
	Payload 2	Non-Geometrical Node	N/A	N/A	N/A	N/A	N/A	N/A	Al_6061
IR Telescope									
	External Structure	Cylinder	0.125	N/A	0.35	1.00E-03	Al_anodized_black	Al_anodized_black	Al_6061
	Disk Structure	Disc	0.125	0.1 r_{min}	N/A	1.00E-03	Black Paint	Black Paint	CFRP
	IR Sensor	Disc	0.07	N/A	N/A	1.00E-03	Goldised_Kapton	CCD_Detector	Silicon
	Telescope Assembly	Cylinder	0.08	N/A	0.225	2.00E-03	Black Paint	Black Paint	CFRP
	Lens	Disc	0.08	N/A	N/A	0.01	IR_lens	IR_lens	Glass
MLI									
	Exterior	Box	0.42	0.32	0.395	1.00E-03	VDA_Kapton	VDA_Kapton	MLI_foil
	Telescope	Cylinder	0.135	N/A	0.34	1.00E-03	VDA_Kapton	VDA_Kapton	MLI_foil
Radiator									
	Instrument radiator	Rectangle	0.25	0.34	N/A	5.00E-03	OSR	OSR	Copper
	CCD radiator	Cone	0.1385 h_{min}	45 ang	0.25 h_{max}	5.00E-03	OSR	OSR	Copper
		Disc	0.1385	N/A	N/A	5.00E-03	OSR	OSR	Copper
	Telescope assembly radiator	Rectangle	0.2	0.2	N/A	1.00E-02	OSR	OSR	Copper
	Structure radiator	Cylinder	0.1385	N/A	0.113333hmax	1.00E-03	OSR	OSR	Copper

Figure 1 and Figures 2 and 3 provide the reader with a visual representation of the geometry of the satellite, as well as the materials and thermo-optical properties that have been assigned to each of its components.

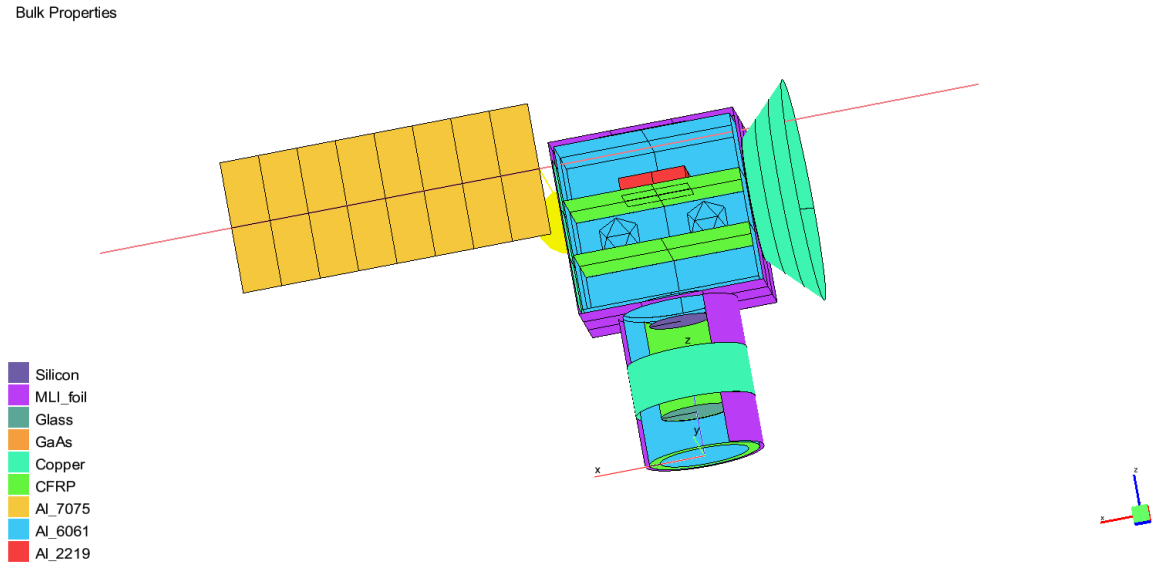

Figure 1: Materials for the passive thermal control system configuration.

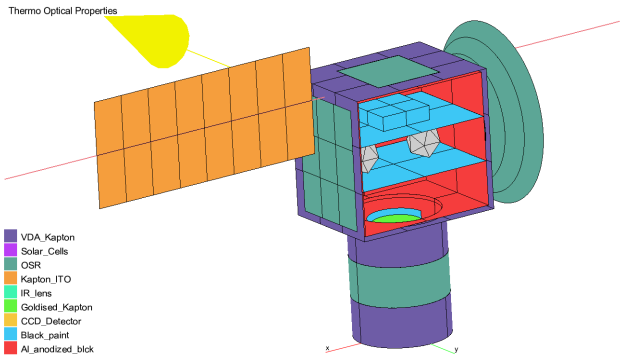

Figure 2: Thermo-optical properties for the passive thermal control system configuration. View 1.

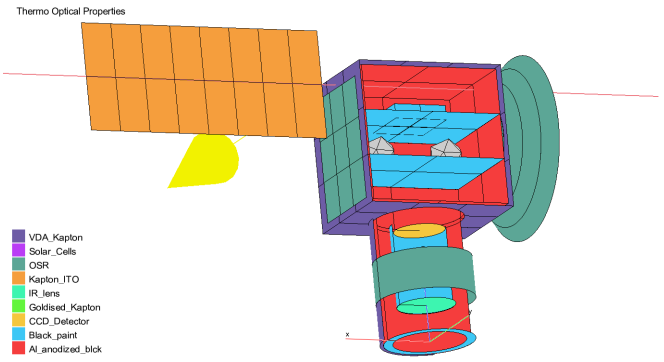

Figure 3: Thermo-optical properties for the passive thermal control system configuration. View 2.

This configuration employs 4 radiators, made of copper material and with the optical solar reflector (OSR) thermo-opctical property applied to their surfaces. This coating provides a minimum solar absorptivity while providing a high IR emissivity which is essential to radiate the heat to the environment. The main radiator, with the conical baffle is used to cool down the CCD through a heat pipe, while the electronic box and the reaction wheels and science experiment are connected through thermal straps. A third cylindrical radiator, placed in the telescope assembly, is used to cool down the lens and telescope structural temperatures. And, finally, a fourth radiator is placed on the top face of the satellite and its used to cool down the structure near the telescope IR sensor.

2.3.2 Conductive interfaces

The correct definition of the conductive interfaces between the elements that compose the satellite is essential to obtain valid results from the simulations. Three types of conductive interfaces have been defined, auto-generated (contact type) conductive interfaces, contact zone interfaces and user-defined conductors (UDC). The first are auto-generated, as the name implies, by ESATAN-TMS, and are shown in Figure 4, whilst the contact zone interface has been defined between the electronic box and the top tray only.

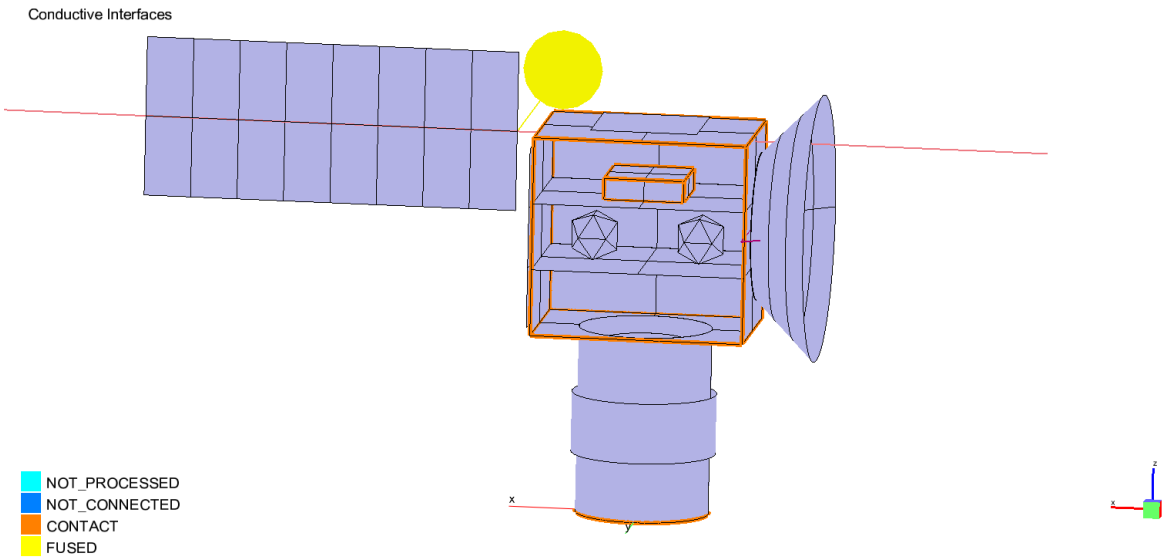

Figure 4: Auto-generated conductive interfaces for the passive thermal control system configuration.

The user-defined conductors, however, must be calculated by the user and given as an input to the software. Three types of interfaces were considered for this task, each representing a different interface type. Table 10 shows the UDCs defined with the use of the following expression:

$$GL_{ij} = \frac{1}{\frac{L_i}{k_i \cdot A_i} + \frac{1}{A_c h_c} + \frac{L_i}{k_j \cdot A_j}}, \tag{1}$$

this is used for the interfaces between the telescope assembly components and the interfaces between the panels and the trays/plates. Table 11 show the GL calculation for the UDCs that represent a conductive interface through a thermal strap or, in the case of the connections between the CCD sensor and its radiator, through a heat pipe. This is calculated through the following expression:

$$\mathrm{GL} = \frac{kA_c}{L}. \tag{2}$$

Finally, the UDCs shown in Table 12 represent the interfaces between the payloads represented by the non-geometrical nodes, the reaction wheels and the on-board science experiment, which is done based on the contact zone formula, hence:

$$\mathrm{GL} = h_c A_c. \tag{3}$$

Table 10: Table showing the GL calculation for the user-defined conductors obtained employing Equation 1. For the case of the satellite configuration with a passive thermal control system.

UDC	**Source**	**Destination**	**Li [m]**	$\mathbf{k}_i$ $[\mathbf{W/(m \cdot}K\mathbf{)}]$	$\mathbf{A}_i$ $[\mathbf{m}^2]$	$\mathbf{A}_c$ $[\mathbf{m}^2]$	$\mathbf{h}_c$ $[\mathbf{W/(m}^2 \cdot K\mathbf{)}]$	$\mathbf{k}_j$ $[\mathbf{W/(m \cdot}K\mathbf{)}]$	$\mathbf{A}_j$ $[\mathbf{m}^2]$	**GL [W/K]**
IR_Tel_Lens_IR_Tel_Obj	IR_Tel_Lens	IR_Tel_Obj	0.081	59	0.00503	4.02124E-05	100	5	4.02E-05	0.001534
IR_Tel_Obj_IR_Tel_CCD	IR_Tel_Obj	CCD	0.08	5	4E-05	1.53938E-05	100	5	1.54E-05	0.000479
IR_Tel_Obj_IR_Tel_STR	IR_Tel_Obj	IR_Tel_STR	0.045	5	4E-05	4.02124E-05	200	160	0.007854	0.002872
IR_Tel_STR_Panel_inf	IR_Tel_STR	Panel_inf	0.13	160	4.9E-05	4.90874E-05	300	160	0.004	0.011812
Panel_Plate_xy	Panel	Plate 1	0.1	160	0.00025	0.00025	100	42	0.0004	0.020639
Panel_Plate_yx	Panel	Plate 1	0.075	160	0.0003	0.0003	100	42	0.0003	0.024481
Panel_Plate2_xy	Panel	Plate 2	0.1	160	0.00025	0.00025	100	42	0.0004	0.020639
Panel_Plate2_yx	Panel	Plate 2	0.075	160	0.0003	0.0003	100	42	0.0003	0.024481
Plate_Panel_xy	Plate 1	Panel	0.1	42	0.0004	0.00025	100	160	0.00025	0.020639
Plate_Panel_yx	Plate 1	Panel	0.075	42	0.0003	0.0003	100	160	0.0003	0.024481
Plate2_Panel_xy	Plate 2	Panel	0.1	42	0.0004	0.00025	100	160	0.00025	0.020639
Plate2_Panel_yx	Plate 2	Panel	0.075	42	0.0003	0.0003	100	160	0.0003	0.024481
IR_Tel_STR_Panel_inf	IR_Tel_STR	Panel_inf	0.13	160	0.00785	0.004	100	160	0.004	0.356306

The values used for determining the GL in Table 10 consider that the interfaces between the structural panels and the instrument trays/plates occurs in the contact area of this two components, which is relatively small. Moreover, the length has been measured from the centre of the origin node to the centre of the destination node and the conductivity values are dependant on the material used for each component. The conductance, h_c, is given a value between 100 and 500 $[\mathrm{W/(m^2 \cdot}K)]$*dependingonhowwellthermallyconnectedthecomponentsare.*

Table 11: Table showing the GL calculation for the user-defined conductors obtained employing Equation 2, that represents the conductance for the thermal straps and heat pipes. For the case of the satellite configuration with a passive thermal control system.

UDC	Source	Destination	k [W/(m·K)]	A_c[m^2]	L [m]	GL [W/K]
CCD_Rad	CCD	Rad_IR_Tel	60000	0.0000350	0.21	10.00000
EBox_Rad	EBox	RAD_INS	1700	0.0007069	0.19	6.32452
IR_Tel_Asmbly_Rad_side	IR_TEL_STR_2	RAD_IR_TEL	1700	0.0003200	0.35	1.55429
IR_Tel_Asmbly_Rad_ext	IR_TEL_STR	RAD_IR_TEL	1700	0.0003200	0.16	3.40000
IR_Tel_Asmbly_RAD_rad_in	IR_TEL_Obj	RAD_IR_TEL	1700	0.0003200	0.05	10.88000
Panel_STR_Rad	Panel	RAD_STR	1700	0.0003200	0.385	1.41299
PLD1_RAD	PLD1	RAD_INS	1700	0.0003200	0.31	1.75484
PLD2_RAD	PLD2	RAD_INS	1700	0.0003200	0.11	4.94545
Panel_SolarPanel	Panel	Solar Panel	160	0.0003142	0.05	1.00531
Rad_disk_V_Rad	Rad_disk	Rad_IR_Tel	1700	0.0003200	0.04	13.60000
RAD_STR_Support	Panel	RAD_STR	5	0.0000283	0.01	0.01414
RAD_IR_Tel_Support	Panel	Rad_IR_TEL	5	0.0000283	0.01	0.01414
RAD_Tel_Support	Panel	Rad_IR_Tel	5	0.0000283	0.01	0.01414
RAD_Ins_Support	Panel	RAD_INS	5	0.0000283	0.01	0.01414

The values used for determining the GL in Table 10 consider that the interface between the CCD and the radiator consists of a heat pipe using Ammonia as working fluid [11]. The equivalent conductivity of the heat pipe was estimated considering the lower bound of the results described in [4], and the contact area has been estimated considering the larger heat pipe standard dimensions provided in [12]. The interfaces between the rest of the components and the radiators use a graphene thermal straps such as those provided by [5], which offer a conductivity of 1700 $\mathrm{W/m \cdot K}$. The interfaces between the solar panels and the structural panels have been calculated considering an Al-6061 cylindrical support structure with a radius of 0.01 m. Finally, the remaining interfaces, that represent the supports for the various radiators are calculated considering the very low thermal conductivity of CFRP, which is the material proposed for this task, resulting in a very low GL, as it is desirable.

Table 12: Table showing the GL calculation for the user-defined conductors obtained employing Equation 3, that represents the conductance for the contact zones between the base of the instruments represented by the non-geometrical nodes. For the case of the satellite configuration with a passive thermal control system.

UDC	Source	Destination	$h_c[W/(m^2 \cdot K)]$	[m^2]	GL [W/K]
Plate2_PLD1	Plate	PLD1	300	0.0036	1.08
Plate2_PLD2	Plate	PLD2	300	0.0049	1.47

2.3.3 Boundary conditions

Another aspect of the thermal design that must be considered is the boundary conditions (BC) that are set for all the components that dissipate heat or require some other type of boundary conditions. Table 13 shows the boundary conditions set for both the nominal and survival modes, for both of the solutions proposed for the thermal design. The BC type temperature corresponds to a set temperature at which a component is kept throughout the simulation. Furthermore, Figure 5 shows the components to which the BCs have been applied to.

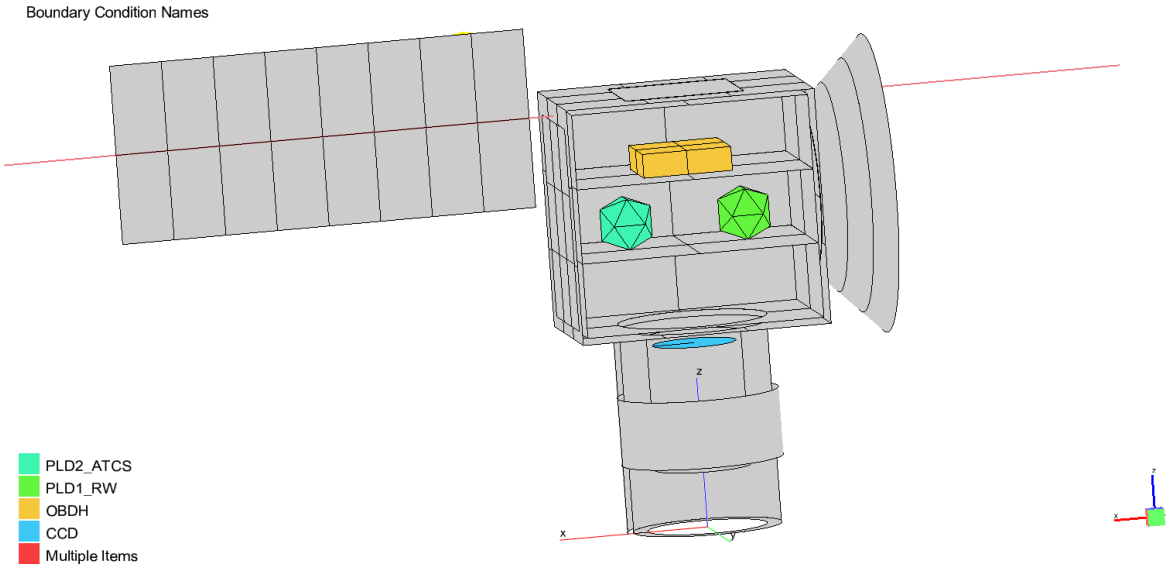

Figure 5: Boundary conditions for the passive thermal control system configuration.

Table 13: Table showing information regarding the boundary conditions (BCs) that have been set for for each of the 2 configurations considered in this study, and for both the nominal and survival operating conditions. The cold case instead is run without setting any boundary conditions to represent all the instrumentation being turned off. Also note that at survival mode the OBDH&C unit operates at half of its power consumption in nominal mode.

Mode	Cooling	PLD1		PLD2		OBDH&C		CCD		Cryo Sink		Cryo Diss	
		BC Type	BC	BC Type	BC	BC Type	BC	BC Type	BC	BC Type	BC	BC Type	BC
Nominal	Passive	Total Heat Area Load	2 W	Total Heat Area Load	4 W	Total Heat Area Load	16 W	Total Heat Area Load	0.15 W	N/A			
	Active + Passive									Temperature	70 K	Total Heat Area Load	16 W
Survival	Passive		0 W		0 W		8 W		0 W	N/A			
	Active + Passive									Temperature	70 K	Total Heat Area Load	0 W

2.3.4 Evolution of the proposed design

The design has undergone a series of changes from its initial design, which consisted of only one traditional radiator for the CCD sensor, to be able to meet the thermal requirements of the mission. The size of the radiators has also changed, with increasingly larger areas with each design iteration, as well as the coating of the back of the CCD sensor, which initially was kept with the same coating as the inferior surface, the one incident to the captured IR radiation, was coated with a Goldised-Kapton finish as to provide minimum IR emissivity.

2.4 ESATAN-TMS micro-satellite model. Active thermal control system configuration

This section aims to provide a detailed description of the proposed configuration which uses an active thermal control system to cool the CCD sensor.

2.4.1 Geometry

The components of the nodes and labels, as well as the geometry, materials and surfaces assigned to each of the elements and sub-elements that compose the satellite model are shown in Table 14 and Table 15 respectively.

Table 14: Table showing the elements and sub-elements that are used for the satellite with a configuration with an active thermal control system . The labels specified in ESATAN-TMS and the nodes that compose each sub-element are shown too.

ELEMENT	SUB-ELEMENT	LABEL	NODE_i	NODE_f
Structure		BODY	10000	19999
	Panels	BODY_PANEL	10000	10999
	Instrument plate	BODY_PLATE_1	11000	11999
	Instrument plate	BODY_PLATE_2	12000	11999
Solar Panels		SPS	20000	29999
	Structure	SPS_STR	20000	20999
	Solar Cells	SPS_CELLS	21000	21999
Instruments		INS	30000	39999
	Electronic Box	INS_EB	30000	30999
	Payload 1	INS_PLD1	31000	31999
	Payload 2	INS_PLD2	32000	32999
IR Telescope		IR_TEL	40000	49999
	Structure	IR_TEL_STR	40000	40999
	Disk Structure	IR_TEL_STR_2	45000	45999
	IR Sensor	IR_TEL_CCD	41000	41999
	Telescope Assembly	IR_TEL_OBJ	43000	43999
	Lens	IR_TEL_LENS	44000	44999
MLI		MLI	50000	59999
	Exterior	MLI_EXT	50000	50999
	Telescope	MLI_IR_TEL	51000	51999
Radiador		RAD	60000	69999
	Instrument radiator	RAD_INS	60000	60999
	CCD radiator	RAD_IR_TEL	61000	61999
		RAD_IR_TEL_2	62000	62999
	Telescope assembly radiator	RAD_IR_Tel_STR	64000	64999
Cryo-cooler		Cryo-Cooler	70000	79000
	Cooled End	Cryo_Sink	70000	71900
	Dissipation End	Cryo_Diss	71000	71999

Table 15: Table showing the geometry that is used to represent the different elements and systems of the satellite, as well as the materials and thermo-optical properties assigned to each geometry. For the case of the active thermal control system for the cryogenic IR telescope CCD sensor.

Element	Sub-element	Shape	Size x [m]	Size y [m]	Size z [m]	Thickness [m]	Surface 1	Surface 2	Material
Estructura									
	Panels	Box	0.4	0.3	0.375	2.00E-03	Al_anodized_black	Al_anodized_black	Al_6061
	Instrument plate	Rectangle	0.4	0.3	N/A	2.00E-03	Black Paint	Black Paint	CFRP
	Instrument plate	Rectangle	0.4	0.3	N/A	2.00E-03	Black Paint	Black Paint	CFRP
Solar Panels		Rectangle	0.936	0.3	N/A	1.00E-03	Solar_cells	Kapton_ITO	GaAs/Al7075
Instruments									
	Electronic Box	Box	0.15	0.15	0.04	2.00E-03	Black Paint	Black Paint	Al_2219
	Payload 1	Non-Geometrical Node	N/A	N/A	N/A	N/A	N/A	N/A	Al_6061
	Payload 2	Non-Geometrical Node	N/A	N/A	N/A	N/A	N/A	N/A	Al_6061
IR Telescope									
	External Structure	Cylinder	0.125	N/A	0.35	1.00E-03	Al_anodized_black	Al_anodized_black	Al_6061
	Disk Structure	Disc	0.125	0.1 r_{min}	N/A	1.00E-03	Black Paint	Black Paint	CFRP
	IR Sensor	Disc	0.07	N/A	N/A	1.00E-03	Goldised_Kapton	CCD_Detector	Silicon
	Telescope Assembly	Cylinder	0.08	N/A	0.225	2.00E-03	Black Paint	Black Paint	CFRP
	Lens	Disc	0.08	N/A	N/A	0.01	IR_lens	IR_lens	Glass
MLI									
	Exterior	Box	0.42	0.32	0.395	1.00E-03	VDA_Kapton	VDA_Kapton	MLI_foil
	Telescope	Cylinder	0.135	N/A	0.34	1.00E-03	VDA_Kapton	VDA_Kapton	MLI_foil
Radiador									
	Instrument radiator	Rectangle	0.25	0.34	N/A	5.00E-03	OSR	OSR	Copper
	CCD radiator	Cone	0.1385 h_{min}	45 ang	0.2 (h_{max})	5.00E-03	OSR	OSR	Copper
		Disc	0.1385	N/A	N/A	5.00E-03	OSR	OSR	Copper
	Telescope assembly radiator	Cylinder	0.1385	N/A	0.113333 h_{max}	1.00E-03	OSR	OSR	Copper
Cryo-cooler									
	Cooled End	Non-Geometrical Node	N/A	N/A	N/A	N/A	N/A	N/A	Al_6061
	Dissipation End	Non-Geometrical Node	N/A	N/A	N/A	N/A	N/A	N/A	Al_6061

Figure 6 and Figures 7 and 8 provide the reader with a visual representation of the geometry of the satellite, as well as the materials and thermo-optical properties that have been assigned to each of its components. It must be noted that the main difference with the solution employing solely the passive thermal control design is the

area of the radiator, which due to the aid of the cryo-cooler can be made smaller, and the use of an added two geometrical nodes to represent the cold and hot ends of the cryo-cooler, with the hot end being the one that dissipates all the power. Therefore, due to the combination of the electronic box and payloads 1 and 2 providing more dissipated power than the cryo-cooler, and since a large radiator is no longer needed to be attached to the CCD for this solution, these instruments are connected, through thermal straps, to the conical-baffle radiator.

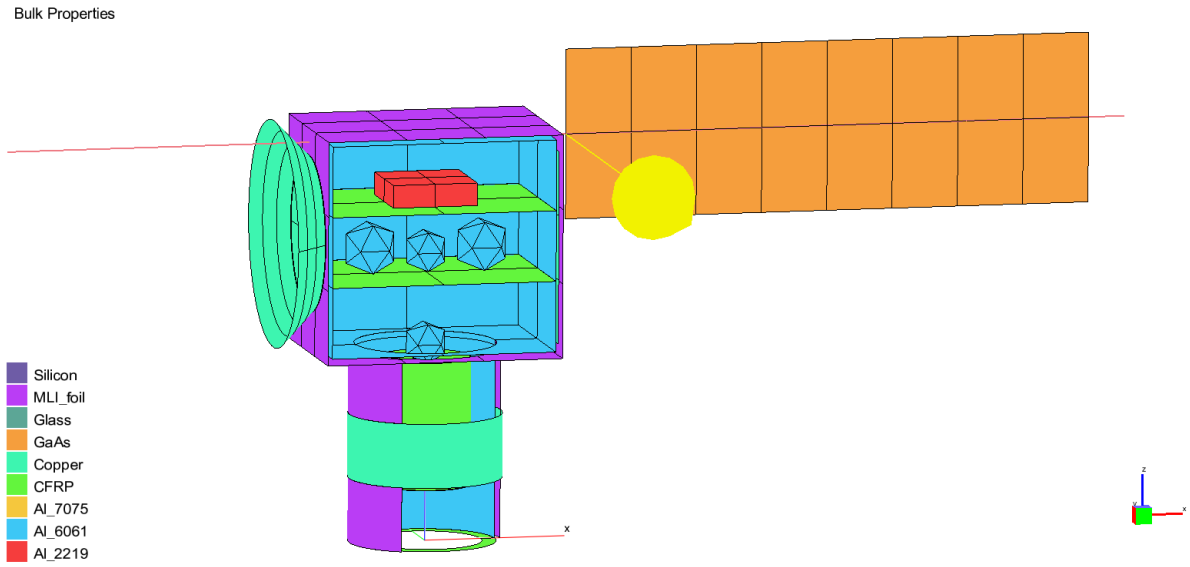

Figure 6: Materials for the active thermal control system configuration.

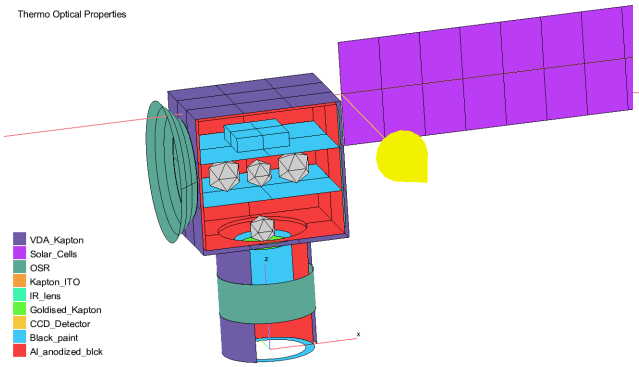

Figure 7: Thermo-optical properties for the active thermal control system configuration. View 1.

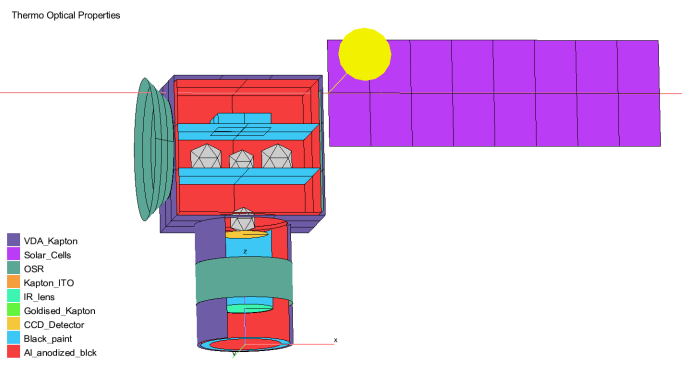

Figure 8: Thermo-optical properties for the active thermal control system configuration. View 2.

This configuration employs 3 radiators, made of copper material and with the optical solar reflector (OSR) thermo-opctical property applied to their surfaces as in the previous configuration. The main radiator, with the conical baffle is used to cool down the electronic box and the reaction wheels and science experiment through a thermal strap interface, and a second radiator, placed on the opposite face, is used to cool down the hot end of the cryo-cooler. A third cylindrical radiator, placed in the telescope assembly, is used to cool down the lens and telescope structural temperatures.

2.4.2 Conductive interfaces

As with the previous proposed solution, three types of conductive interfaces have been defined, auto-generated (contact type) conductive interfaces, contact zone interfaces and user-defined conductors (UDC). The first are auto-generated, as the name implies, by ESATAN-TMS, and are shown in Figure 9, whilst the contact zone interface has been defined between the electronic box and the top tray, and both sides of the hot end of the cryo-cooler and the bottom tray.

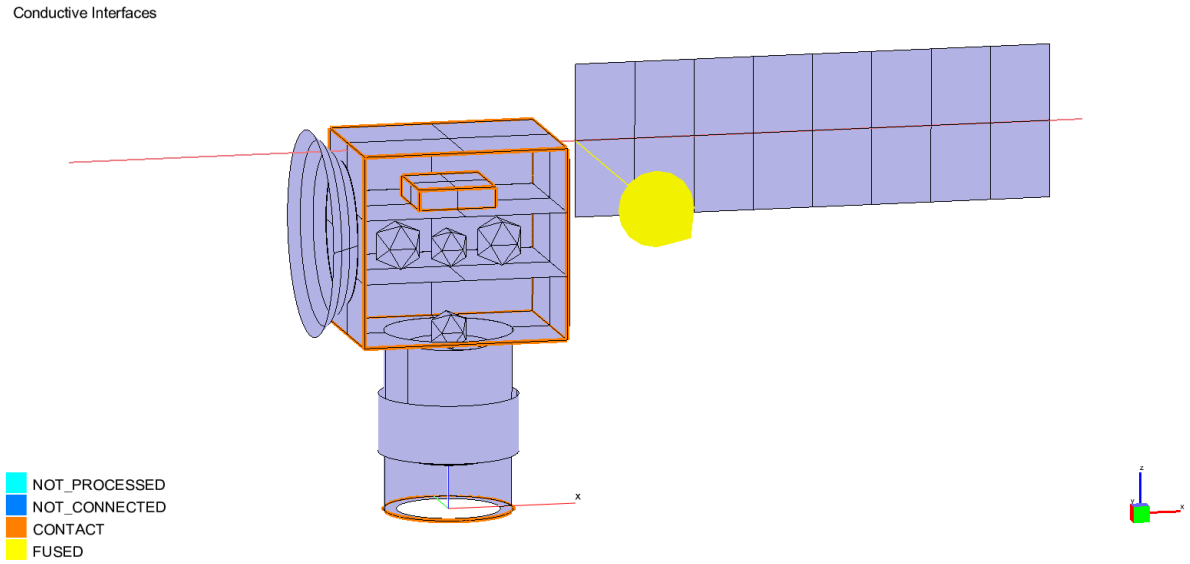

Figure 9: Auto-generated conductive interfaces for the active thermal control system configuration.

Table 16 shows the UDCs defined with the use of Equation 1. This is used for the interfaces between the telescope assembly components and the interfaces between the panels and the trays/plates. Table 17 show the GL calculation for the UDCs that represent a conductive interface through a thermal strap or, in the case of the connections between the CCD sensor and its radiator, through a heat pipe. This is calculated through Equation 2. Finally, the UDCs shown in Table 18 represent the interfaces between the payloads represented by the non-geometrical nodes, the reaction wheels and the on-board science experiment, which is done based on Equation 3.

Table 16: Table showing the GL calculation for the user-defined conductors obtained employing Equation 1. For the case of the satellite configuration with an active thermal control system.

UDC	Source	Destination	Li [m]	k_i [W/(m $\cdot K$)]	A_i [m^2]	A_c [m^2]	h_c [W/($m^2 \cdot K$)]	k_j [W/(m $\cdot K$)]	A_j [m^2]	GL [W/K]
IR_Tel_Lens_IR_Tel_Obj	IR_Tel_Lens	IR_Tel_Obj	0.081	59	0.00503	4.02124E-05	100	5	4.02E-05	0.001534
IR_Tel_Obj_IR_Tel_CCD	IR_Tel_Obj	CCD	0.08	5	4E-05	1.53938E-05	100	5	0.000015	0.000479
IR_Tel_Obj_IR_Tel_STR	IR_Tel_Obj	IR_Tel_STR	0.045	5	4E-05	4.02124E-05	200	160	7.85E-03	0.002872
IR_Tel_STR_Panel_inf	IR_Tel_STR	Panel_inf	0.13	160	4.9E-05	4.90874E-05	300	160	4.00E-03	0.011812
Panel_Plate_xy	Panel	Plate 1	0.1	160	0.00025	0.00025	100	42	4.00E-04	0.020639
Panel_Plate_yx	Panel	Plate 1	0.075	160	0.0003	0.0003	100	42	3.00E-04	0.024481
Panel_Plate2_xy	Panel	Plate 2	0.1	160	0.00025	0.00025	100	42	4.00E-04	0.020639
Panel_Plate2_yx	Panel	Plate 2	0.075	160	0.0003	0.0003	100	42	3.00E-04	0.024481
Plate_Panel_xy	Plate 1	Panel	0.1	42	0.0004	0.00025	100	160	2.50E-04	0.020639
Plate_Panel_yx	Plate 1	Panel	0.075	42	0.0003	0.0003	100	160	3.00E-04	0.024481
Plate2_Panel_xy	Plate 2	Panel	0.1	42	0.0004	0.00025	100	160	2.50E-04	0.020639
Plate2_Panel_yx	Plate 2	Panel	0.075	42	0.0003	0.0003	100	160	3.00E-04	0.024481
IR_Tel_STR_Panel_inf	IR_Tel_STR	Panel_inf	0.13	160	0.00785	0.004	100	160	0.004	0.356306

The values used for determining the GL in Table 16 follow a similar procedura as what is stated in Section 2.3.

Table 17: Table showing the GL calculation for the user-defined conductors obtained employing Equation 2, that represents the conductivity for the thermal straps and heat pipes. For the case of the satellite configuration with an active thermal control system.

UDC	Source	Destination	k [W/(m·K)]	A_c[m^2]	L [m]	GL [W/K]
EBox_Rad	EBox	RAD_INS	1700	0.0007069	0.19	6.32452
IR_Tel_Asmbly_Rad_side	IR_TEL_STR_2	RAD_IR_TEL	1700	0.0003200	0.35	1.55429
IR_Tel_Asmbly_Rad_ext	IR_TEL_STR	RAD_IR_TEL	1700	0.0003200	0.16	3.40000
IR_Tel_Asmbly_RAD_rad_in	IR_TEL_Obj	RAD_IR_TEL	1700	0.0003200	0.05	10.88000
PLD1_RAD	PLD1	RAD_INS	1700	0.0003200	0.31	1.75484
PLD2_RAD	PLD2	RAD_INS	1700	0.0003200	0.11	4.94545
Panel_SolarPanel	Panel	Solar Panel	160	0.0003142	0.05	1.00531
Rad_disk_V_Rad	Rad_disk	Rad_IR_Tel	1700	0.0003200	0.04	13.60000
RAD_IR_Tel_Support	Panel	Rad_IR_TEL	5	0.0000283	0.01	0.01414
RAD_Tel_Support	Panel	RAD_IR_TEL	5	0.0000283	0.01	0.01414
RAD_Ins_Support	Panel	RAD_INS	5	0.0000283	0.01	0.01414
CCD_to_CryoCool_Sink	CCD	Cryocooler sink	1700	0.0000785	0.02	6.67588
CryoCool_Sink_Support	Cryocooler Sink	RAD_IR_STR	5	0.0000785	0.125	0.00314
CryoCool_Diss_RAD	Cryocooler Diss	Rad_IR_Tel	1700	0.0003142	0.21	2.54319

The values used for determining the GL in Table 17 consider that the interfaces between the instruments and the radiators use a graphene thermal straps such as those provided by [5], which offer a conductivity of 1700 $W/m \cdot K$. The interfaces between the solar panels and the structural panels have been calculated considering an Al-6061 cylindrical support structure with a radius of 0.01 m. Finally, the remaining interfaces, that represent the supports for the various radiators are calculated considering the very low thermal conductivity of CFRP, which is the material proposed for this task, resulting in a very low GL, as it is desirable.

Table 18: Table showing the GL calculation for the user-defined conductors obtained employing Equation 3, that represents the conductivity for the contact zones between the base of the instruments represented by the non-geometrical nodes. For the case of the satellite configuration with an active thermal control system.

UDC	Source	Destination	$h_c[W/(m^2 \cdot K)]$	[m^2]	GL [W/K]
Plate2_PLD1	Plate1	PLD1	300	0.0036	1.08
Plate2_PLD2	Plate1	PLD2	300	0.0049	1.47
CryoCool_Diss_Support	Plate1	Cryocooler diss	100	0.0025024	0.12512

2.4.3 Boundary conditions

Table 13 shows the boundary conditions set for both the nominal and survival modes, for both of the solutions proposed for the thermal design. The BC type temperature corresponds to a set temperature at which a component is kept throughout the simulation. Furthermore, Figure 10 shows the components to which the BCs have been applied to.

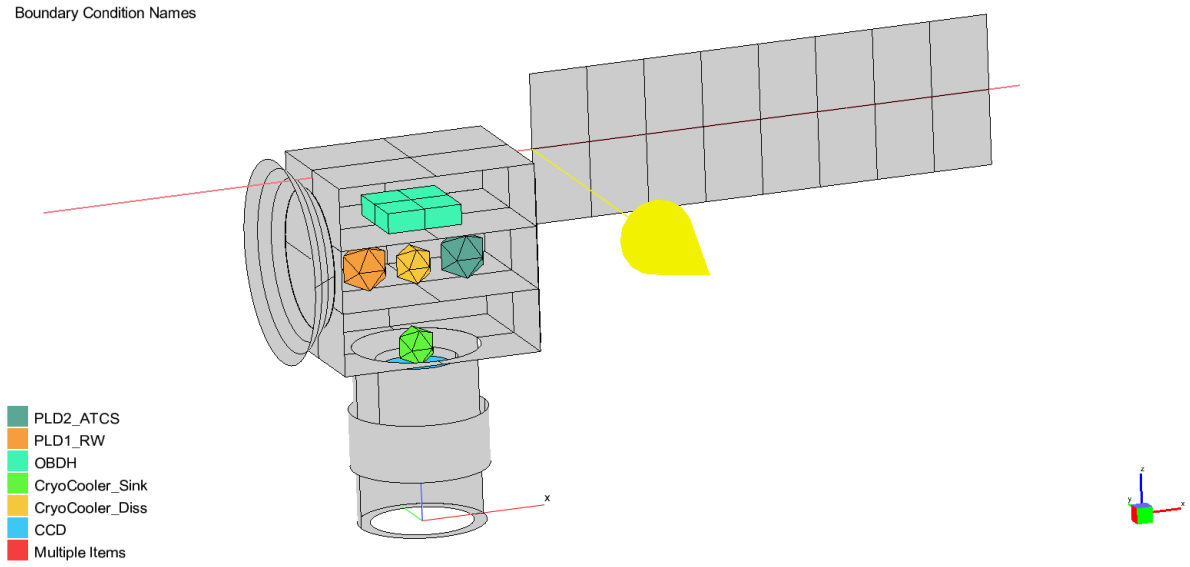

Figure 10: Boundary conditions for the active thermal control system configuration.

3 Results

This section aims to provide the results obtained from the thermal simulations for both of the proposed configurations. A detailed review on the temperatures of the various components and how this compares to their operational temperature range is also provided, along with a series of graphs depicting the evolution of the temperature of the satellite and its components throughout the duration of the orbit.

3.1 ESATAN-TMS micro-satellite model. Orbit

With the resolution of the radiative case, the total incident radiation on the solar panels can be determined, and, therefore, the average incident solar radiation, shown in Figure 11, can be used to determine the total power generated, and hence, with the aid of this information, the solar panels were resized accordingly so that the produced power equals the dissipated power. This is essential for the correct development of the analysis case. It must be noted that since for both configurations the orbit is the same the average incident solar radiation is also the same.

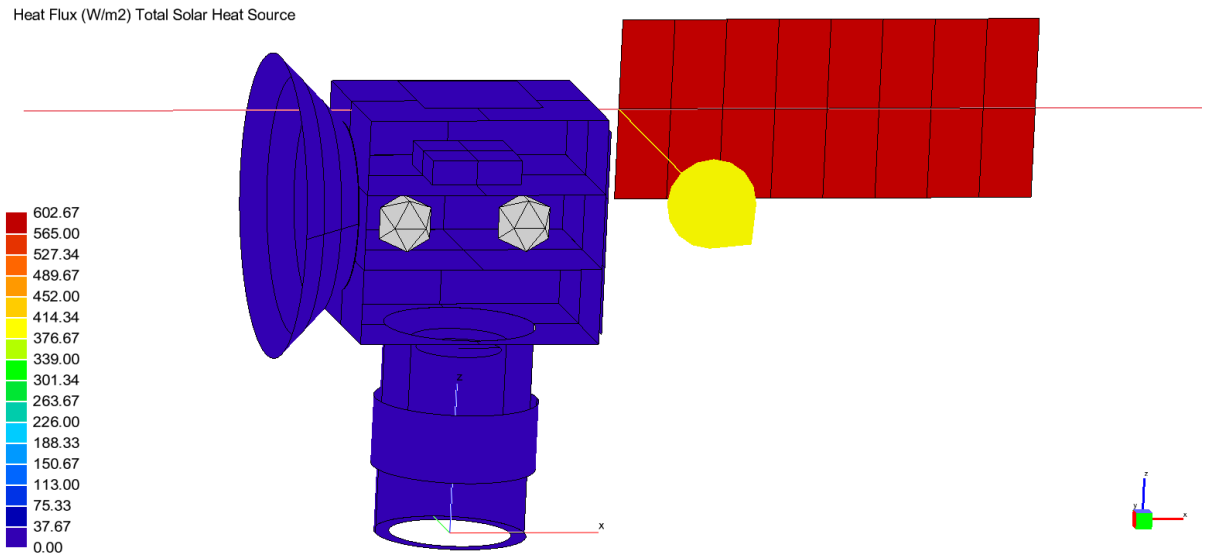

Figure 11: Average Heat Flux for the LEO SS 12am orbit.

3.2 ESATAN-TMS micro-satellite model. Passive thermal control system configuration

The results of the thermal analysis for the passive thermal control configuration are given in this section.

3.2.1 Nominal operational mode

The first results that are presented are given for the satellite in its nominal operational mode. Figure 12 and Figures 13 to 16 show the temperature throughout the orbit at various points of the structure and for various components. The satellite is presented with a cut on some of its components as to provide a view of the interior. It can be seen how the hottest areas are the top part of the square section of the satellite, as well as the solar panels, with the coldest parts being the telescope assembly, and especially, the CCD.

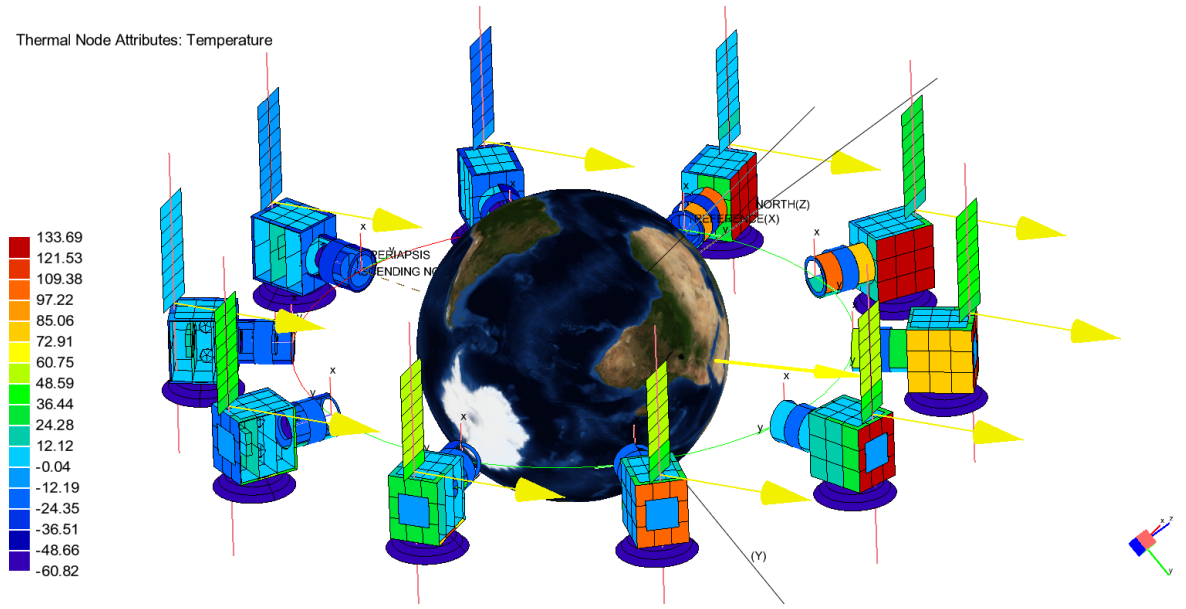

Figure 12: Micro-satellite temperature throughout the SS 12am orbit for passive thermal control system configuration.

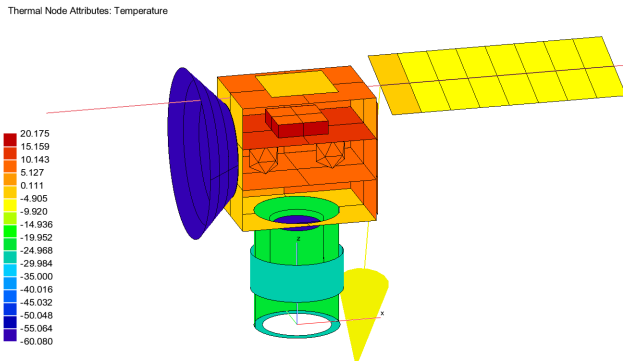

Figure 13: Micro-satellite temperature at an instant of the SS 12am orbit for passive thermal control system configuration. At $t = 0.00$ s.

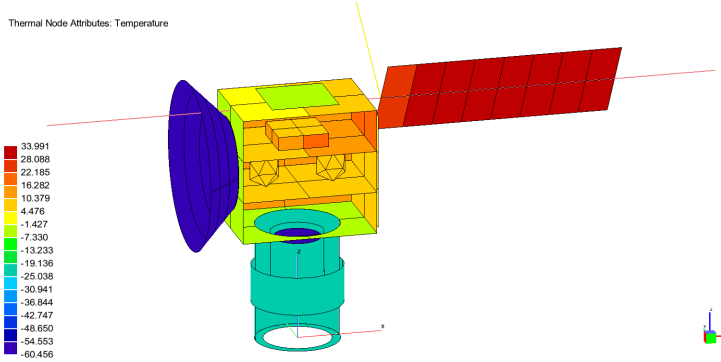

Figure 14: Micro-satellite temperature at an instant of the SS 12am orbit for passive thermal control system configuration. At $t = 1817.79$ s.

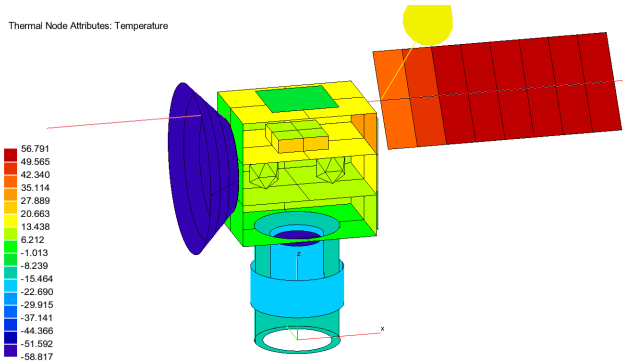

Figure 15: Micro-satellite temperature at an instant of the SS 12am orbit for passive thermal control system configuration. At $t = 3635.57$ s.

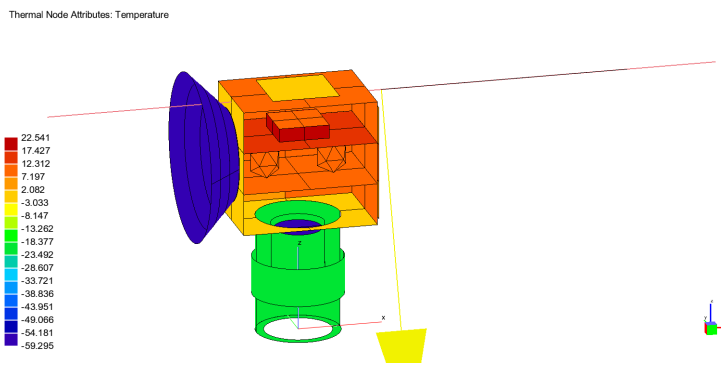

Figure 16: Micro-satellite temperature at an instant of the SS 12am orbit for passive thermal control system configuration. At $t = 5453.36$ s.

In order to visualise the evolution of the temperature of the components and structural elements at various points of the orbit the following graphs are presented. Figure 17 shows the evolution of the temperature of the electronic box (cotaining the OBDH sub-system), the reaction wheels (PLD2) and the science experiment (PLD1). As expected, since the electronic box dissipates a larger amount of power, its temperatures is higher than that of the other payloads. However, they are all well into their operational limits.

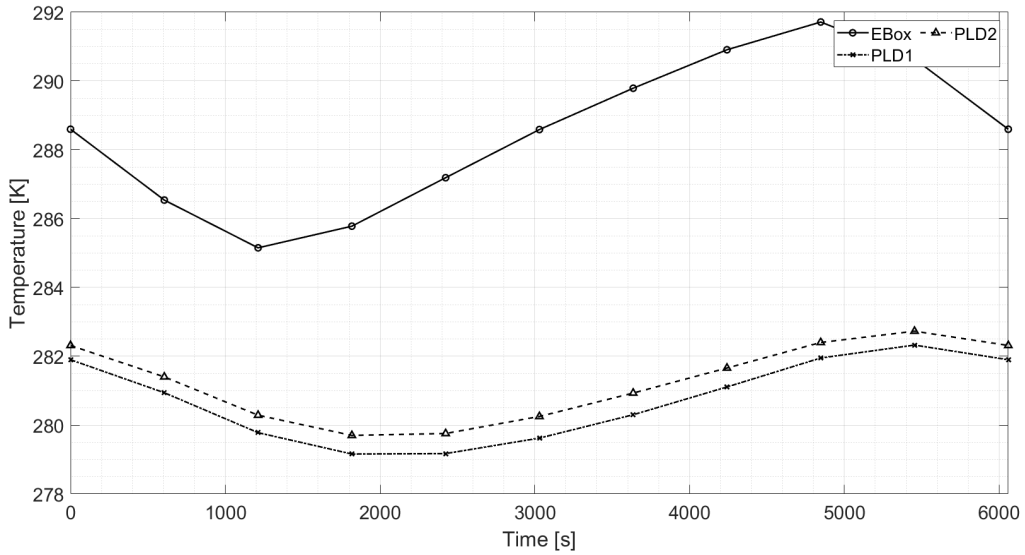

Figure 17: Instrumentation temperature throughout the SS 12am orbit for passive thermal control system configuration.

Figure 18 shows the evolution of the temperature of the solar panels, the structural panels, the telescope lens and the telescope objective assembly. It can be seen that the temperature of the lens and telescope objective assembly, cooled by the same radiator that cools the telescope structure is kept almost constant, as it is in the shadow at all times. On the contrary, the temperature of the panels varies greatly throughout the orbit, as it is exposed to both direct sun and parts of eclipse. The panel temperature also shows some variation along the orbit, likely due to the heat transferred from the MLI or the solar panel interface assembly.

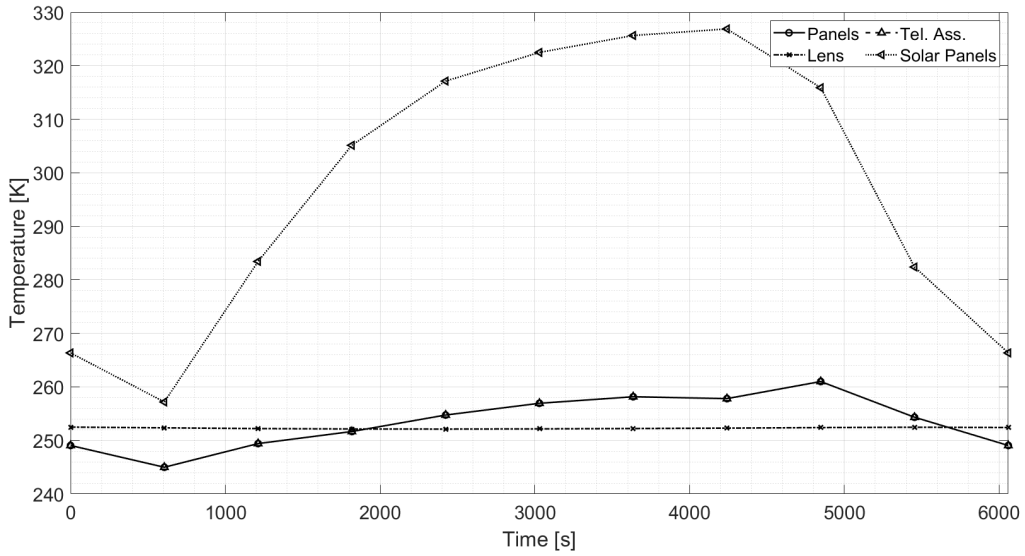

Figure 18: Temperature of various structural components of the micro-satellite throughout the SS 12am orbit for passive thermal control system configuration.

Figure 19 shows the CCD temperature variation, which is of just under 2.5 K, which results in a very stable temperature sensor which is desirable.

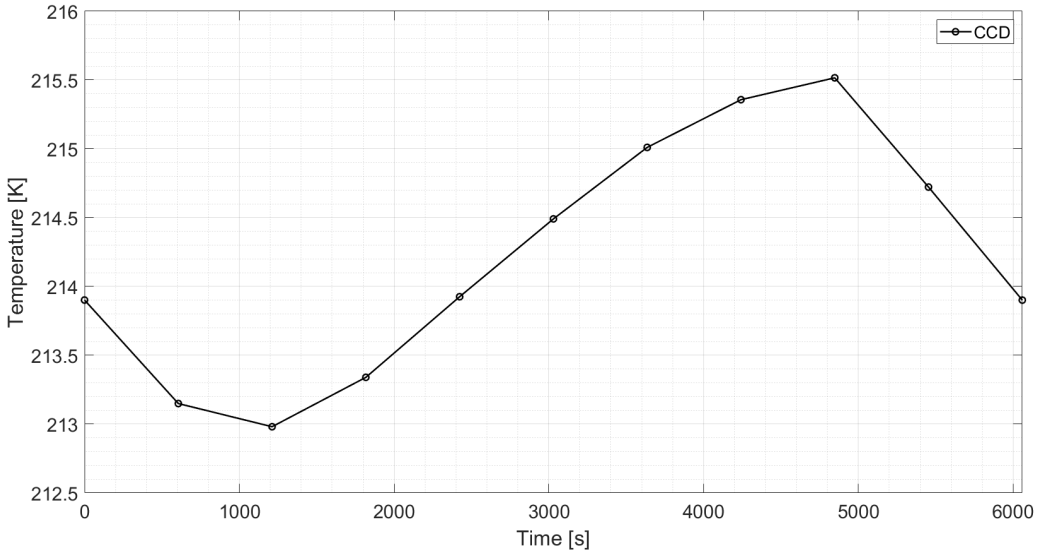

Figure 19: Temperature of the CCD detector throughout the SS 12am orbit for passive thermal control system configuration.

Finally, Figure 20 shows the heat flow (in Watts) from various components to others through the conductive interfaces, throughout the SS 12am orbit for passive thermal control system configuration. A negative heat flow represents heat flowing from the first component to the second. For example, for the case of the *EBox-Rad* curve, which shows the heat flow between the electronic box and its radiator, it can be seen how a maximum of almost 10 W are transfered to the radiator during some parts of the orbit. It can be seen how for the case of the heat flow from the solar panels to the structural panels the values become positive for parts of the orbit, this corresponds from moments where heat flows from the structural panels to the solar panels as these become really cool in the

eclipse area, whilst the structural panels maintaina a more constant temperature since they are shielded by the MLI blankets.

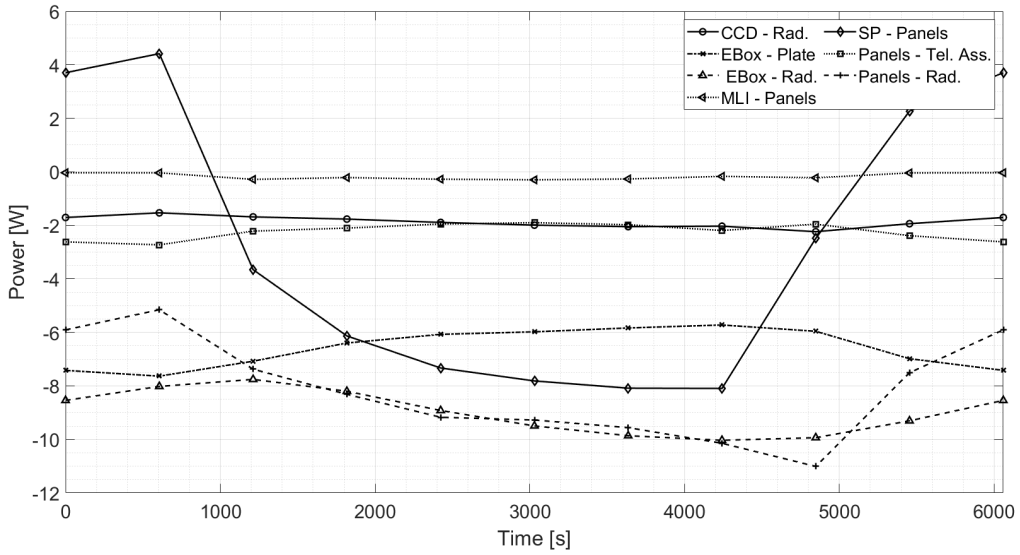

Figure 20: Heat flow from various components to others through the conductive interfaces, throughout the SS 12am orbit for passive thermal control system configuration.

3.2.2 Survival operational mode

Figure 21 shows the temperature variation of the electronic box, the CCD, the reaction wheels (PLD2) and the science experiment (PLD1) throughout the orbit. It can be seen how the temperatures are considerably lower than those in the nominal mode, but the instruments remain within their operational limits.

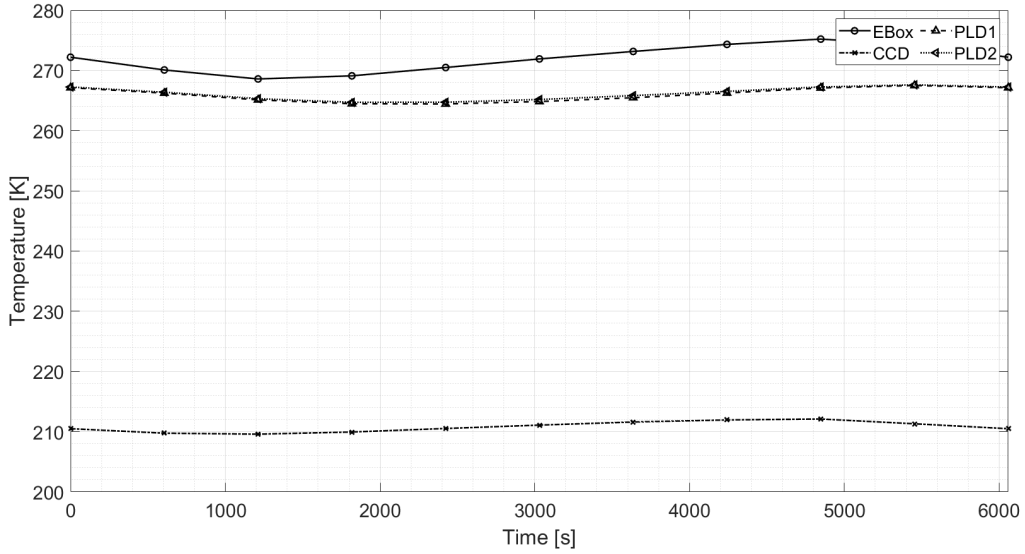

Figure 21: Instrumentation temperature throughout the SS 12am orbit for passive thermal control system configuration. Survival mode.

3.2.3 Cold case

Figure 22 shows the same temperature of the same components as in Figure 21, but for the cold case, in which no power is dissipated. The temperatures reach even lower values than in the survival mode, but despite this the components remain safely within the operational limits, although close to the lower limits for the case of the reaction wheel and science instrument.

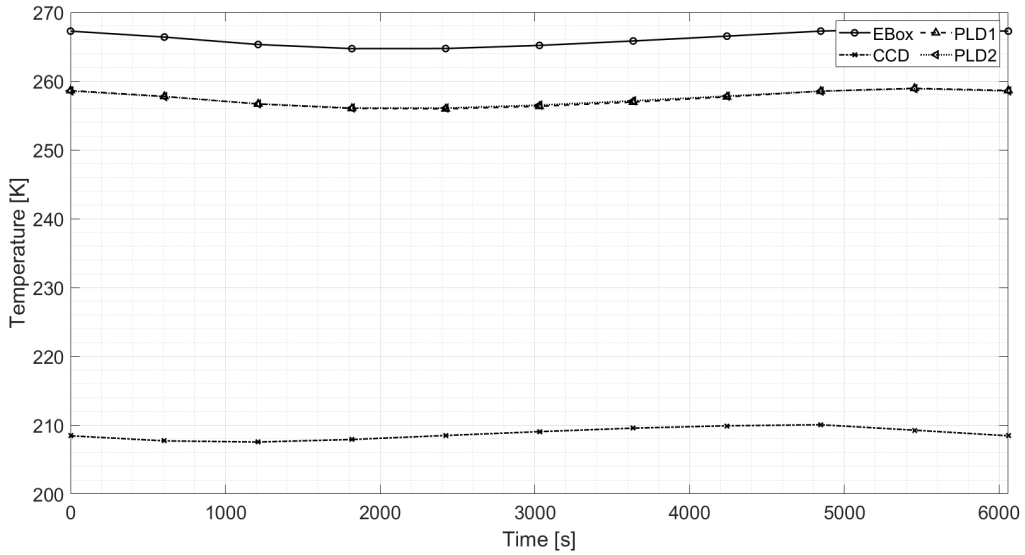

Figure 22: Instrumentation temperature throughout the SS 12am orbit for passive thermal control system configuration. Cold case (all instruments are turned off).

3.3 ESATAN-TMS micro-satellite model. Active thermal control system configuration

The results of the thermal analysis for the active thermal control configuration are given in this section.

3.3.1 Nominal operational mode

The first results that are presented are given for the satellite in its nominal operational mode. Figure 23 and Figures 24 to 27 show the temperature throughout the orbit at various points of the structure and for various components. The satellite is presented with a cut on some of its components as to provide a view of the interior. It can be seen how the hottest areas are the top part of the square section of the satellite, as well as the solar panels. It can also be seen how the CCD and cold side of the cryo-cooler remain at a costant temperature of 70 K.

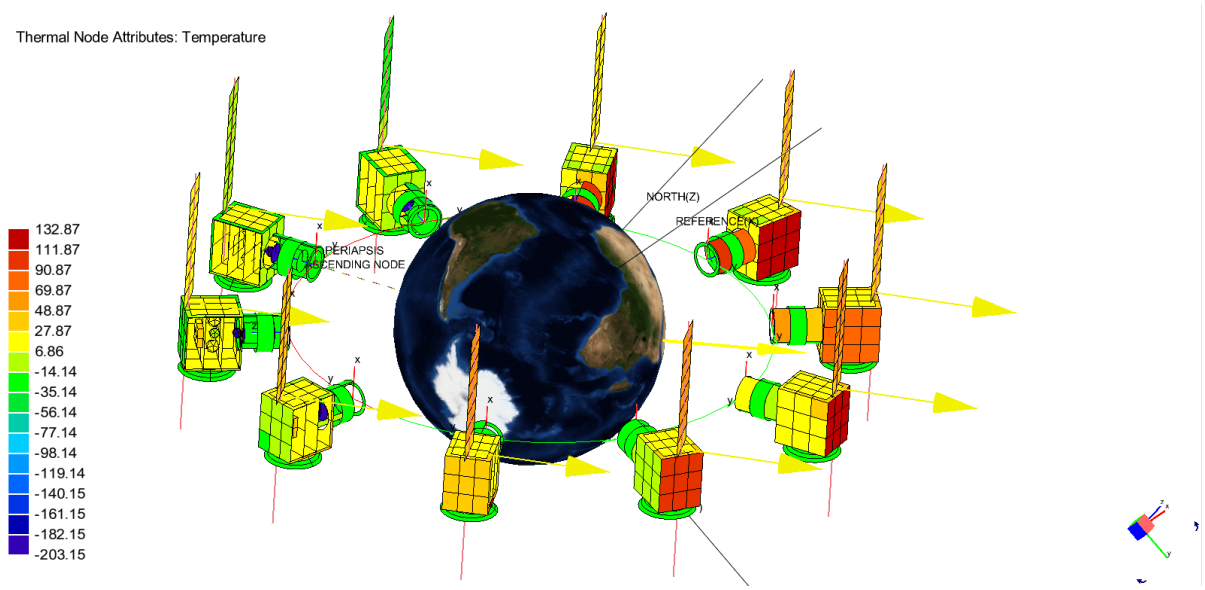

Figure 23: Micro-satellite temperature throughout the SS 12am orbit for active thermal control system configuration.

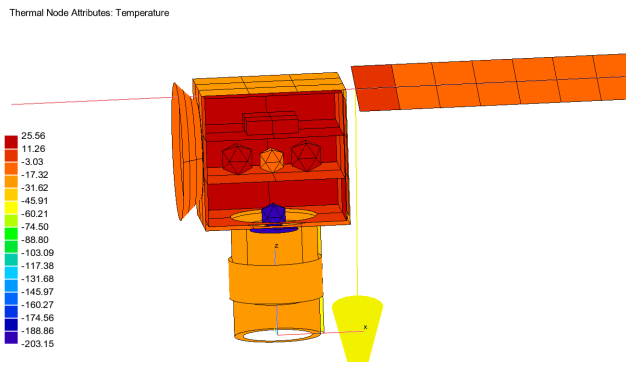

Figure 24: Micro-satellite temperature at an instant of the SS 12am orbit for active thermal control system configuration. At $t = 0.00$ s.

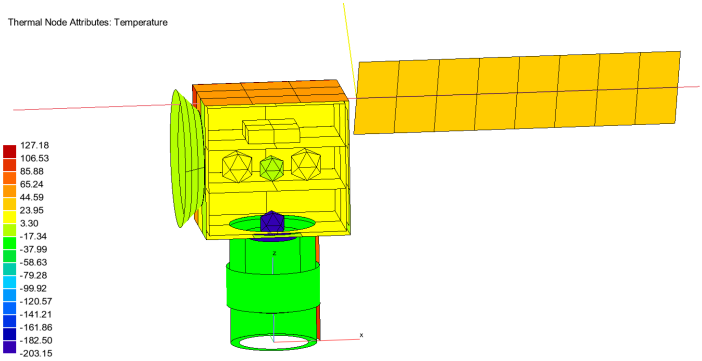

Figure 25: Micro-satellite temperature at an instant of the SS 12am orbit for active thermal control system configuration. At $t = 1817.79$ s.

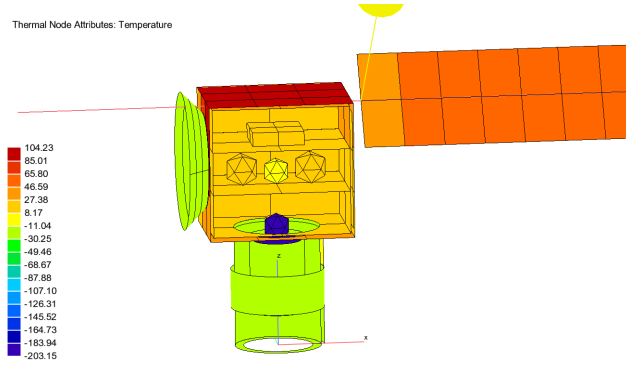

Figure 26: Micro-satellite temperature at an instant of the SS 12am orbit for active thermal control system configuration. At $t = 3635.57$ s.

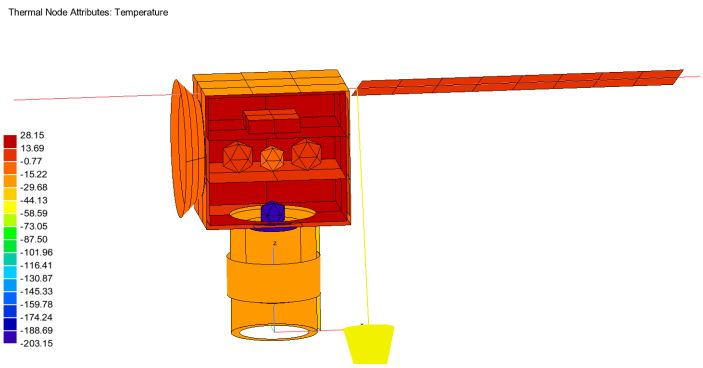

Figure 27: Micro-satellite temperature at an instant of the SS 12am orbit for active thermal control system configuration. At $t = 5453.36$ s.

In order to visualise the evolution of the temperature of the components and structural elements at various points of the orbit the following graphs are presented. Figure 28 shows the evolution of the temperature of the electronic box (cotaining the OBDH sub-system), the reaction wheels (PLD2) and the science experiment (PLD1). As expected, since the electronic box dissipates a larger amount of power, its temperatures is higher than that of the other payloads. However, they are all well into their operational limits.

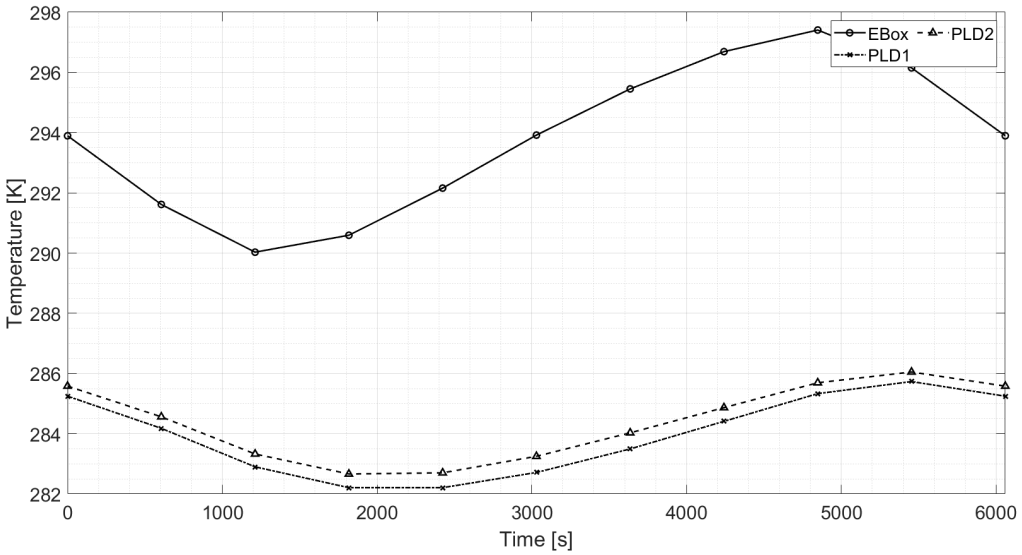

Figure 28: Instrumentation temperature throughout the SS 12am orbit for active thermal control system configuration.

Figure 29 shows the evolution of the temperature of the solar panels, the structural panels, the telescope lens and the telescope objective assembly. It can be seen that the temperature of the lens and telescope objective assembly, cooled by the same radiator that cools the telescope structure is kept almost constant, as it is in the shadow at all times. On the contrary, the temperature of the panels varies greatly throughout the orbit, as it is exposed to both direct sun and parts of eclipse. The panel temperature also shows some variation along the orbit, likely due to the heat transferred from the MLI or the solar panel interface assembly.

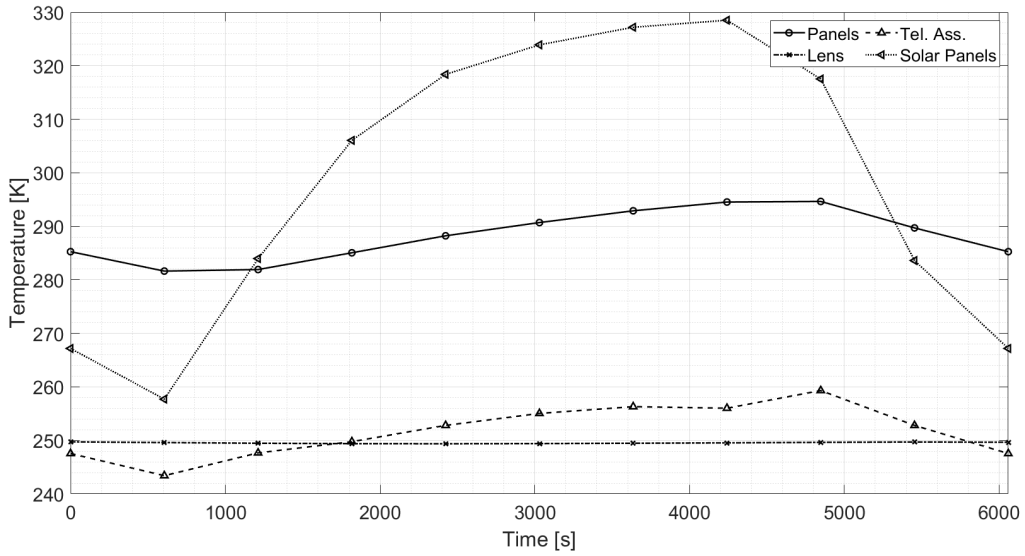

Figure 29: Temperature of various structural components of the micro-satellite throughout the SS 12am orbit for active thermal control system configuration.

Figure 30 shows the CCD temperature variation, which is of just under 2.5 K, which results in a very stable temperature sensor which is desirable.

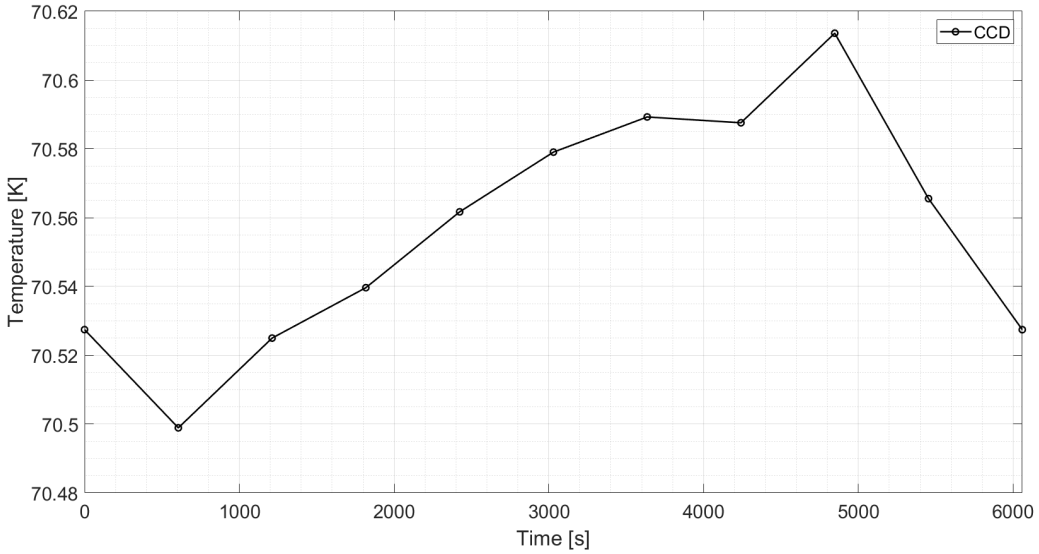

Figure 30: Temperature of the CCD detector throughout the SS 12am orbit for active thermal control system configuration.

Finally, Figure 20 shows the heat flow (in Watts) from various components to others through the conductive interfaces, throughout the SS 12am orbit for passive thermal control system configuration. It can be seen how a large amount of heat flows from the various payloads to their radiator. This power is, as expected lower than their total dissipated power, as the rest is radiated to the environment or transferred through conduction to other elements of the satellite.

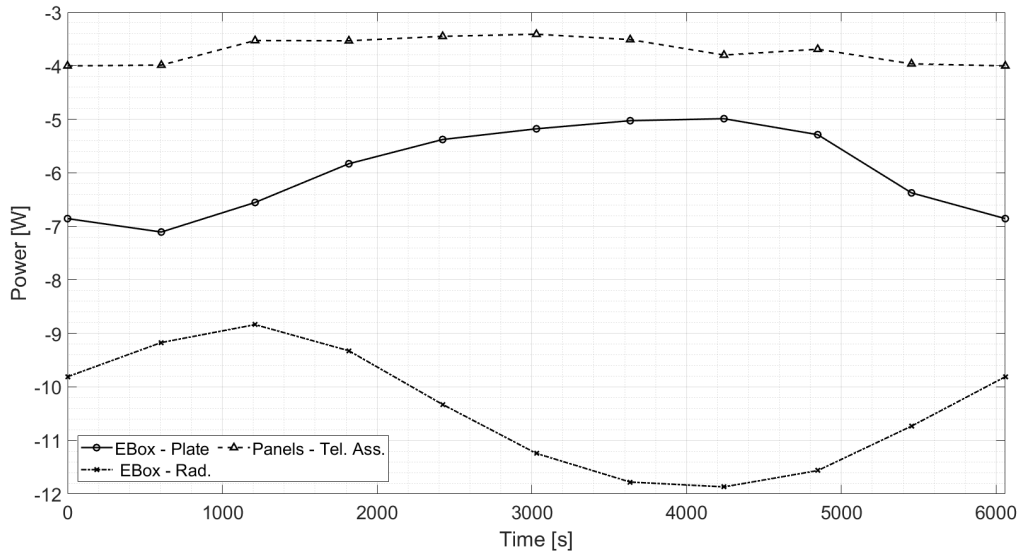

Figure 31: Heat flow from various components to others through the conductive interfaces, throughout the SS 12am orbit for active thermal control system configuration.

3.3.2 Survival operational mode

Figure 32 shows the temperature variation of the electronic box, the CCD, the reaction wheels (PLD2) and the science experiment (PLD1) throughout the orbit. It can be seen how the temperatures are considerably lower than those in the nominal mode, but the instruments remain within their operational limits. t can be seen that since the cryo-cooler is turned off under this operational mode, the temperatures of the CCD sensor increases up to around 250 K.

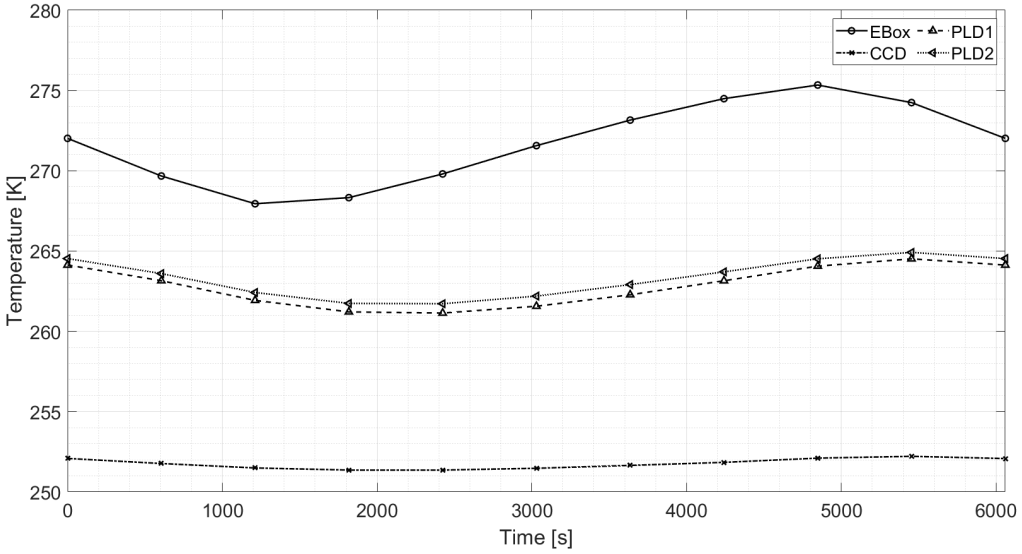

Figure 32: Instrumentation temperature throughout the SS 12am orbit for active thermal control system configuration. Survival mode.

3.3.3 Cold case

Figure 22 shows the temperature variation of the electronic box, the CCD, the reaction wheels (PLD2) and the science experiment (PLD1) throughout the orbit for the cold case, in which no power is dissipated. The temperatures reach even lower values than in the survival mode, but despite this the components remain safely within the operational limits, although close to the lower limits for the case of the reaction wheel and science instrument.

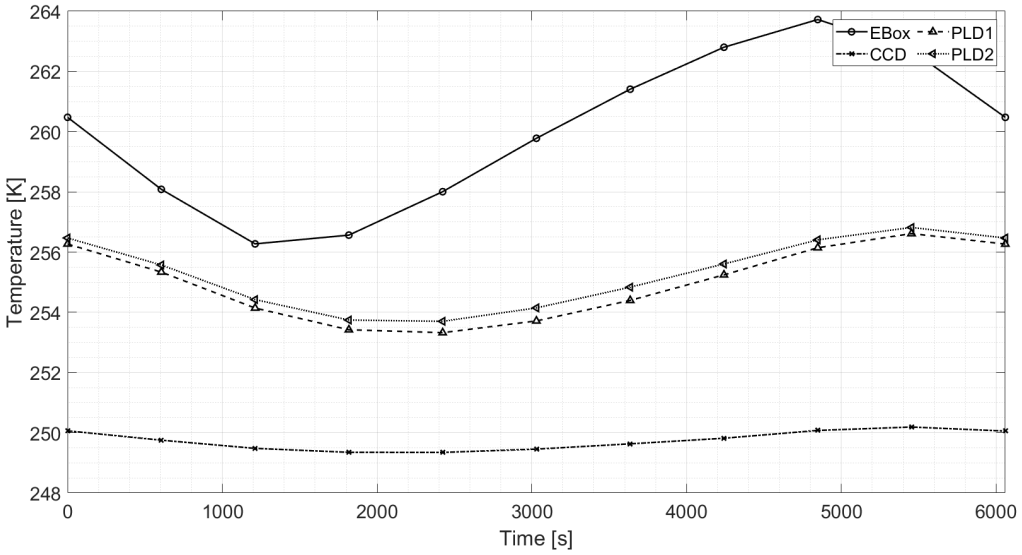

Figure 33: Instrumentation temperature throughout the SS 12am orbit for active thermal control system configuration. Cold case (all instruments are turned off).

3.4 Comparison of the proposed design configurations

Finally a series of comparison tables are provided with the intent to provide the reader with an overview of the performance of both configurations and their advantages and disadvantages with respect to each other. Firstly, Table 19 shows the maximum and minimum temperatures of the CCD, reaction wheels (PLD2), science experiment (PLD1) and electronic box (OBDH) encountered under the nominal and survival operational modes for both of the configurations proposed: the totally passive thermal control system and the thermal control system that employs an active cryo-cooler to maintain the CCD under cryogenic conditions. The upper and lower bounds of the design temperatures for each component is also provided. As it can be seen, all requirements are met.

Table 19: Comparison between the instrumentation temperatures in the nominal and survival modes, for each configuration proposed. Namely, the passive and active thermal control system configurations.

Mode	**Thermal Control System**	CCD Temperature [K]		CCD Operating Temperature [K]		PLD1 Temperature [K]		PLD1 Operating Temperature [K]		PLD2 Temperature [K]		PLD2 Operating Temperature [K]		OBDH&C Temperature [K]		OBDH&C Operating Temperature [K]	
		Max.	Min.	Max.	Min.	Max.	Min.	Max.	Min.	Max.	Min.	Max.	Min.	Max.	Min.	Max.	Min.
Nominal	Passive	215.5	213.0	323	153	282.3	279.2			282.7	279.7			291.7	285.2		
	Active + Passive	70.6	70.5	110	60	285.7	282.2	253.2	333.2	286.1	282.7	343.15	233.15	297.4	290	338.15	248.15
Survival	Passive	212.1	209.6	323	153	267.5	264.4			267.6	264.7			275.2	268.6		
	Active + Passive	252.2	251.4	110	60	264.5	261.1			264.9	261.7			275.3	267.9		

In Table 20 shows a comparison between the instrumentation temperatures in the nominal mode, for the passive and active thermal control system configurations proposed. Information regarding the total radiator area, total solar panel area, power and CCD model and manufacturer is also provided.

Table 20: Comparison between the instrumentation temperatures in the nominal mode, for the passive and active thermal control system configurations proposed.

Thermal Control System	**Radiators**	**Total Radiator Area** [m^2]	**Total Solar Panel Area** [m^2]	**Active Thermal Control**	**Power [W]**	**CCD Temperature [K]**		**Detector model**	**Detector Operating Temp. Range [K]**		**Source**
						Max.	Min.		Max.	Min.	
Passive	4	0.2839	0.21	NO	22.1	215.5	213.0	e2V CCD290-99	323	153	[6]
Active +Passive	3	0.2439	0.28	Cryo-cooler	38.1	70.60	70.50	PICNIC IR detector	110	60	[8]

Furthermore, in Table 21 a comparison between the instrumentation temperatures in the survival mode and cold case modes, for each configuration proposed. Namely, the passive and active thermal control system configurations. The minimum payload temperature for each component is also provided, and as it can be seen, the temperatures are within the desired range.

Table 21: Comparison between the instrumentation temperatures in the survival mode and cold case cases, for each configuration proposed. Namely, the passive and active thermal control system configurations.

Case	Thermal Control System	Radiators	Active Thermal Control	Nominal Power [W]	Total Dissipated Power [W]	Heaters	Minimum Payload Temperature [K]		
							PLD1	PLD2	OBDH&C
Survival Mode	Passive	4	N/A	22.1	2	NO	264.4	264.7	268.6
	Active+Passive				0	NO	261.1	261.7	267.9
Cold Case	Passive	3	Cryo-cooler	38.1	2	NO	256.0	256.1	264.7
	Active+Passive				0	NO	253.3	253.7	256.3

3.5 Short comment on the chosen orbit

It must be noted that the type of sun-synchronous orbit chosen plays a key role on the thermal design of the satellite. In the case of the chosen orbit, a sun-synchronous 12 am orbit at 800 km, the areas of the satellite that receive direct solar radiation are not the same throughout the orbit, which helps distribute the heat around the satellite. However, if a sun-synchronous 6 am orbit was to be chosen, the solar radiation would be incident always on the same face of the satellite. This could have posed an advantage in the thermal control for this mission as the telescope assembly and radiators could be kept in the shadow at all times which could have helped to achieve a passive thermal control system capable of reaching cryogenic temperatures for the CCD. It is encouraged that future studies consider this. However, this type of orbit also poses problems as one side of the satellite would get considerably hotter than the other. Figures 34 and 35 show the temperature distribution for the passive and active thermal designs respectively in a SS 6 am orbit. As it can be seen, a number of design changes should be made as to maintain the radiators out of the incident solar radiation, since the results obtained are worse than those obtained for the SS 12 am orbit. Furthermore, the average solar radiation incident to the panels also changes, as they are not at the shadow at any point, which therefore, would require modifications to the solar panel area.

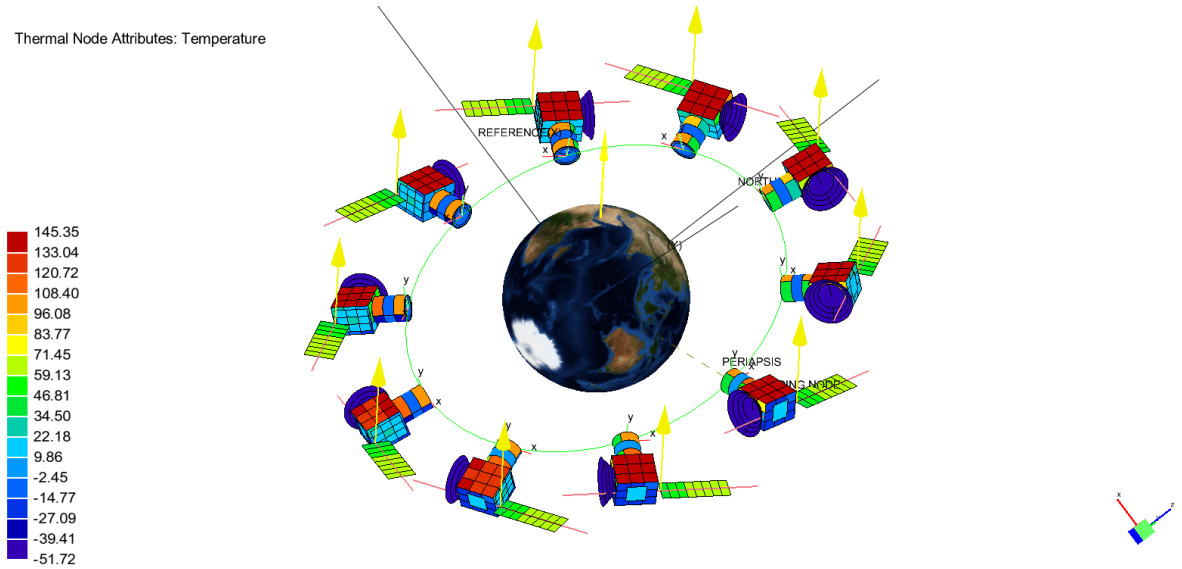

Figure 34: Micro-satellite temperature throughout the SS 6am orbit for passive thermal control system configuration.

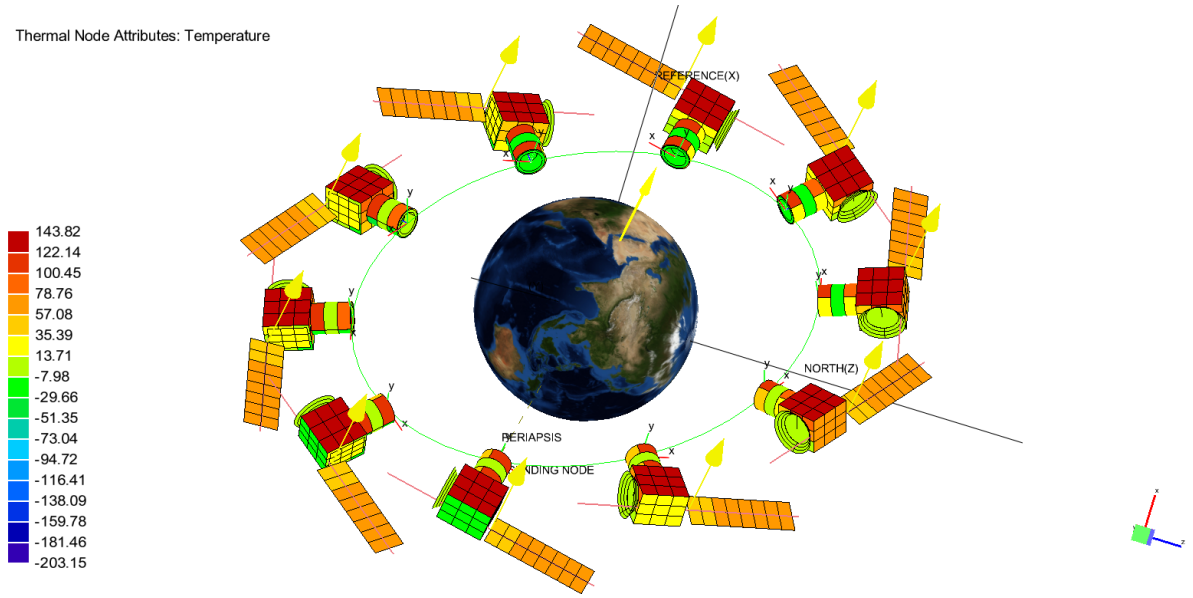

Figure 35: Micro-satellite temperature throughout the SS 6am orbit for active thermal control system configuration.

4 Conclusions

This study has carried out the preliminary design for an earth-observation (EO) satellite in low-earth sun-synchronous (SS) circular orbit. Two designs were studied, a completely passive thermal design and an active thermal design using a cryo-cooler for the CCD sensor.

Regarding the choice between both of the configurations proposed, the configuration employing a passive thermal control system to maintain the CCD at a temperature of around 215 K is encouraged due to the lower risk, cost and complexity that come with the use of active thermal control devices such as the cryo-cooler employed for

the second configuration. For situations in which the non-cryogenically cooled CCD produces sufficient quality readings, with noise levels within the requirements, this should be the obvious choice. The second configuration, however, becomes necessary if, due to the noise requirements on the sensor readings, cryogenic temperatures are required.

In conclusion, this study has shown how the ESATAN-TMS software can be used for developing the preliminary-design of a micro-satellite, with it being an easy tool to iterate various design configurations and obtain some first approximation simulation results. The effect of various types of thermal control systems, along with the effect of the orbit on such system and the choice of materials and thermo-optical properties have been studied.

References

[1] Blue Canyon Technologies, Reaction Wheels Products, Tech. rep.

[2] Endurosat, Onboard Computer (OBC) — CubeSat by EnduroSat.
URL https://www.endurosat.com/cubesat-store/cubesat-obc/onboard-computer-obc/

[3] Ricor, Ricor Cryocooler Product Catalogue.
URL https://www.ricor.com/wp-content/uploads/2019/07/RicorComparisonTable2019.pdf

[4] B. Mehta, M. Soni, K. Changela, Review of Parametric Investigation of Cryogenic Heat Pipe, Tech. Rep. 2 (2014).

[5] Thermal Space, Thermal LyNX graphene thermal straps have superior thermal efficiency and flexibilityThermal Space.
URL https://thermal-space.com/thermal-lynx/

[6] E2V, CCD290-99 Back Illuminated Scientific CCD Sensor.

[7] W. Han, D.-H. Lee, W.-S. Jeong, Y. Park, B. Moon, S.-J. Park, J. Pyo, I.-J. Kim, W.-K. Park, D. Lee, K.-I. Seon, U.-W. Nam, S.-M. Cha, K. Park, J.-H. Park, I.-S. Yuk, C. Hee Ree, H. Jin, S. Choel Yang, H.-Y. Park, G.-H. Shin, J.-K. Seo, S.-W. Rhee, J.-O. Park, H. Mok Lee, H. Murakami, T. Matsumoto, MIRIS: A Compact Wide-field Infrared Space Telescope, Publications of the Astronomical Society of the Pacific 126 (943) (2014) 853–862. doi:10.1086/678130.

[8] European Space Agency, Sixth European Symposium on Space Environmental Control Systems, Tech. rep.
URL https://earth.esa.int/documents/10174/1598482/GEN90.pdf

[9] MatWeb, Search Capabilities for Materials Property Data.
URL http://www.matweb.com/search/search.aspx

[10] I. Martínez, THERMO-OPTICAL PROPERTIES, Tech. rep.
URL http://webserver.dmt.upm.es/$\sim$isidoro/dat1/Thermooptical.pdf

[11] Boyd Corporation, Cryogenic Heat Pipes — Boyd Corporation.
URL https://www.boydcorp.com/thermal/two-phase-cooling/cryogenic-heat-pipes.html

[12] I. T. C. Team, Control Térmico Espacial - Heat Pipes.
URL https://moodle.upm.es/titulaciones/oficiales/pluginfile.php/1628898/mod_resource/content/2/6%20HeatPipes.pdf